A shock-wave model for periodic-wave transformation and energy dissipation in the inner surf zone

P. Bonneton*
Department of Geology and Oceanography, UMR CNRS EPOC,
University of Bordeaux I, 33405 Talence, France.

Abstract

In this paper, we revisit the nonlinear shallow water shock-wave model and its ability to predict wave distortion and energy dissipation of periodic broken waves in the inner surf zone. We extend the classical presentation of nonlinear shallow water weak solutions (Stoker (1957)), by taking into account non-flat bottom and friction effects. From this shock-wave approach, which is more general than the classical bore model (Svendsen et al. (1978)) generally used in coastal engineering, we derive time-averaged equations. In particular, from time-averaging of the non-conservative momentum equation, we obtain a new equation to predict wave setup in the inner surf zone. This equation gives the setup as a function of the broken-wave energy dissipation. We also derive a new one-way time-dependent model for predicting the transformation of non-reflective broken waves. This one-way model can represent

*p.bonneton@epoc.u-bordeaux1.fr

an useful alternative to the classical bore model. Finally, we compare numerical simulations of both, the nonlinear shallow water shock-wave model and the simplified one-way model, with spilling wave breaking experiments and we find a good agreement. These results show, in particular, that the kinematics and the energy dissipation of periodic broken waves in the inner surf zone are well predicted by weak solutions of the nonlinear shallow water equations.

Keywords: Surf zone; Nonlinear shallow water equations; Saint Venant equations; Broken-wave; Shock-wave; Weak solution; Energy dissipation ; One-way equation

1 Introduction

As the waves propagate shoreward to gradually smaller depth, their height and steepness increase, until they break. The dominant types of breakers in natural sandy beaches are spilling and plunging breakers (Galvin (1968) and Peregrine (1983)). In spilling breakers, the wave crest becomes unstable and spills down the front part of the wave, producing a foamy water surface. In plunging breakers, the crest curls over the shoreward face of the wave and crashes into the base of the wave, causing a large splash. In both cases, immediately after the initiation of breaking a rapid change in the wave shape occurs, in a region that has been named the "transition region" (Svendsen et al. (1978)). Shoreward of this region the wave field changes more slowly and reorganizes itself into quasi-periodic bore-like waves. This region, which extends to the shoreline where the run-up starts, has been termed the "inner surf zone" (ISZ). As noticed by Svendsen et al. (1978), one of the remarkable features of the ISZ is that the broken waves from a plunging breaker cannot be visually distinguished from those originating from a spilling breaker. Shoreward of the ISZ, the swash zone is the area which is intermittently covered and uncovered by wave run-up. In this paper we consider conditions for which the surf zone has a significant ISZ, and then beaches of sufficiently gentle uniformly varying slopes.

The classical approach for ISZ-wave modelling is based on the depth-integrated momentum and energy equations time-averaged over a wave period (e.g. Hamm et al. (1993) for a review). Wave height and setup variations are computed from integral wave properties, such as the energy flux, the radiation stress, and the energy dissipation. These models are relatively simple and useful for practical applications except in the swash zone. However, in some applications, e.g. sediment transport modelling, the prediction of time-varying quantities, such as the ISZ oscillating velocities or swash oscillations, is required. In this paper, we revisit the time-dependent nonlinear shallow water (NSW) shock-wave model and its ability to predict periodic broken-wave transformation in the ISZ.

The NSW shock-wave approach, extensively used in hydraulics problems (Stoker (1957) and Whitham (1974)), has been successfully applied for studying single bore propagation on a beach. For instance, one-way analytical solutions of this phenomenon were first given by Whitham (1958) and Ho and Meyer (1962), and numerical simulations were performed by Keller et al. (1960) and Hibberd and Peregrine (1979). On the other hand, only few theoretical NSW-based studies have been devoted to the dynamics of periodic (or quasi-periodic) broken waves propagating in the ISZ.

Kobayashi and his colleagues (Kobayashi et al. (1987, 1989, 1990 and 1996)) developed a shock-capturing numerical NSW model, and showed that it gives good results in comparison with laboratory measurements of periodic ISZ broken waves. Using a similar modelling approach, Raubenheimer et al. (1996) and Bonneton et al. (2000 and 2005) found a good agreement between computed ISZ wave solutions and field observations on gently sloping beaches. However, in spite of these promising results, the validity of the NSW equations for describing wave distortion and energy dissipation in the ISZ, is frequently challenged. For instance, Liu et al. (1991) wrote the following comment: "Interestingly, even though many assumptions of the shallow-water wave theory are violated in the surf zone, certain quantitative and qualitative comparisons of its predictions with the experimental or field data often produce good agreement: this is puzzling". The main objectives of this paper are to shed some light on this problem and to evaluate to what extent the NSW shock-wave approach describes adequately the time-dependent ISZ broken-wave transformation. We will also discuss the ability of this shock-wave model, which corresponds to a more general approach than the classical bore model (Svendsen et al. (1978), to give a theoretical framework to evaluate time-averaged quantities such as energy dissipation and wave setup.

The paper is outlined as follows. A detailed analysis of the validity of NSW hypotheses in the ISZ is given in section 2. In sections 3, we derive NSW shock-wave solutions, extending the classical presentation (Stoker (1957)) by taking into account non-flat bottom and friction effects. From this shock-wave approach we derive time-averaged equations for periodic broken waves propagating in the ISZ. Using the shock-wave theory, we derive in section 4 a new one-way model to predict the transformation of non-reflective periodic broken waves. Finally in section 5, validity of both NSW and one-way shock-wave solutions is assessed from comparisons with laboratory ISZ experiments.

2 Validity of NSW hypotheses in the inner surf zone

In this section, after a brief introduction of the NSW shock-wave model, we will analyze the validity of the NSW approximations for describing periodic-wave transformation in the ISZ.

2.1 NSW equations and shock-wave concept

We consider two-dimensional broken-wave propagation in the vertical plane (x, z), where x is the horizontal coordinate and z the vertical coordinate taken to be positive upward, with $z = 0$ at the still water level. In the ISZ, the broken-wave wavelength is very large compared to both the water depth and the wave front width. To reduce the dimension and number of unknowns of this shallow water problem, a vertical integration of the Navier Stokes equations can be performed over the instantaneous water depth $h(x, t)$. Using the kinematic and dynamic boundary conditions at both the bottom, $z = -d(x)$, and the free surface, $z = \zeta(x, t)$, we can obtain the following depth-integrated equations (e.g. Dingemans (1997))

$$\frac{\partial h}{\partial t} + \frac{\partial hu}{\partial x} = 0 \tag{1}$$

$$\rho \frac{\partial hu}{\partial t} + \rho \frac{\partial}{\partial x}\left(hu^2 + \frac{1}{2} g h^2\right) - \rho g h \frac{\partial d}{\partial x} = -\tau^b + \frac{\partial T^\nu}{\partial x} + \frac{\partial V}{\partial x} + N \ , \tag{2}$$

where $u = \frac{1}{h}\int_{-d}^{\zeta} v_1 \ dz$ is the depth-averaged horizontal velocity, v_1 the horizontal velocity component, g the gravitational acceleration, ρ the fluid density, τ^b the bottom-shear stress, and

$$T^\nu = 2\rho\nu \int_{-d}^{\zeta} \frac{\partial v_1}{\partial x} \ dz \ ,$$

$$V = \int_{-d}^{\zeta} -\rho \tilde{u}^2 \, dz \quad , \quad \text{with} \quad \tilde{u} = v_1 - u \quad ,$$
$$N = \frac{\partial}{\partial x}\left(\int_{-d}^{\zeta} -p \, dz\right) + p(-d)\frac{\partial d}{\partial x}$$

where ν is the kinematic viscosity, p the dynamic pressure defined by $p(x, z, t) = P(x, z, t) - \rho g(\zeta(x, t) - z)$ and P the pressure. T^{ν} is the integrated viscous stress, V the excess momentum flux due to both turbulence and vertical non-uniformity of the velocity profile, and N characterizes non-hydrostatic effects.

It is important at this point to emphasize that the only approximations that have been made in the derivation of these equations are related to the air-water interface hypotheses: air entrainment and surface tension can be neglected and ζ is a single-valued function of x.

Depth-integrated equations (1) and (2) cannot be evaluated any further unless theoretical or empirical closure relations are introduced for terms on the right-hand side of the horizontal momentum equation (2). By neglecting the three last terms and using a standard bottom friction parameterization quadratic in u we obtain the NSW equations with friction (also named Saint Venant equations)

$$\frac{\partial h}{\partial t} + \frac{\partial hu}{\partial x} = 0 \tag{3}$$
$$\rho\frac{\partial hu}{\partial t} + \rho\frac{\partial}{\partial x}\left(hu^2 + \frac{1}{2}gh^2\right) - \rho g h\frac{\partial d}{\partial x} = -\frac{1}{2}\rho f_r |u| u \ , \tag{4}$$

where the friction coefficient f_r is about 10^{-2} in the ISZ.

The classical demonstration of the NSW equations (e.g. Stoker (1957)) assumes that vorticity and vertical acceleration are negligibly small, and that any variations of surface level ζ or of depth-averaged velocity u have a length-scale λ_0 many times the characteristic water depth d_0. Despite these strong assumptions, comparisons with both large-scale laboratory data and field data have demonstrated a remarkable capability of the NSW equations to predict the complex dynamics of long waves in the nearshore (e.g. Liu et al. (1991)). The most surprising feature is the ability of these equations to describe broken-wave propagation in the ISZ (e.g. Kobayashi et al. (1989), Raubenheimer et al. (1996) or Bonneton et al. (2005)), despite intense vorticity and vertical acceleration observed in such flows.

In fact, vorticity and vertical acceleration are strongly localized, and we can schematically distinguish two regions in ISZ broken waves (see figure 1a): a thin "wave front" (WF) where the flow variables change rapidly, and a "regular wave region" (RWR).

In the upper part of WF, the turbulent region of recirculating water carried with the wave is called the "roller" region. WF are characterized by non-hydrostatic pressure deviations and strongly vertically non-uniform velocity distributions (see Govender et al. (2002)). Laboratory experiments performed by Nadaoka et al. (1989) and Ting and Kirby (1996) have shown that turbulence and energy dissipation are mainly located in WF.

Conversely, in RWR, as shown by Ting and Kirby (1996) and Lin and Liu (1998), horizontal velocity is nearly vertically uniform, pressure distribution is almost hydrostatic, vorticity and turbulence intensities are weak.

The underlying hypotheses for the NSW equations seem, therefore, to be satisfied for RWR and not for the thin WF. Moreover, it is well known (Stoker (1957)) that in most cases the NSW equations, with or without friction, result in discontinuous solutions (shocks), which can be considered as the mathematical counterparts of WF. In this paper we will consider that the ISZ-wave solution can be approximated by introducing discontinuities (see figure 1b) satisfying appropriate shock conditions (see section 3) and retaining the NSW equations in continuous parts of the flow (RWR).

2.2 Scaling analysis

To examine the approximations involved in the NSW equations we present a scaling analysis of depth-integrated equations (1) and (2). We consider periodic broken waves propagating in the ISZ and we restrict our analysis to RWR.

The scales of the variables are suggested by the long wave theory. The length scales that characterize wave motion are λ_0, a_0 ($H_0 = 2a_0$ is the characteristic wave height), and d_0, which are the typical values of wavelength, free-surface amplitude and water depth. The time scale is λ_0/c_0, where $c_0 = (gd_0)^{1/2}$. The characteristic scales for velocity and dynamic pressure are given respectively by $\mathcal{U} = a_0 c_0/d_0$ and $\mathcal{P} = \rho g a_0 d_0^2/\lambda_0^2$. Characteristic scales for the integrated viscous stress term may be estimated as $\rho\nu\mathcal{U}d_0/\lambda_0$.

To distinguish the turbulent contribution from the contribution of the vertical non-uniformity of the wave velocity we introduce the operator $\langle . \rangle$ which is an ensemble average. The horizontal x-component of the velocity field v_1 can be decomposed into two parts: the ensemble-averaged velocity $\langle v_1 \rangle$, which is the organized wave-induced velocity including both undertow and orbital wave motion, and turbulent velocity fluctuations $v_1' = v_1 - \langle v_1 \rangle$. Using the decomposition $\tilde{u} = (\langle v_1 \rangle - u) + v_1'$ and neglecting interaction between $\langle v_1 \rangle - u$ and v_1', V can be expressed as:

$$V = V^t + \tilde{V}$$

where $V^t = \int_{-d}^{\zeta} -\rho v_1'^2 \, dz$ is the excess momentum flux due to turbulence and $\tilde{V} = \int_{-d}^{\zeta} -\rho(\langle v_1 \rangle - u)^2 \, dz$ the excess momentum flux due to vertical non-uniformity of the velocity profile. The characteristic scales for V^t and $\tilde{V}$ are given respectively by $\mathcal{V}^t$ and $\tilde{\mathcal{V}}$.

Let us normalize all variables according to the scales anticipated on physical grounds:

$$\begin{aligned}
x_a &= \frac{x}{\lambda_0} \qquad \zeta_a = \frac{\zeta}{a_0} \qquad t_a = \frac{t}{\lambda_0/c_0} \qquad z_a = \frac{z}{d_0} \\
d_a &= \frac{d}{d_0} \qquad p_a = \frac{p}{\mathcal{P}} \qquad u_a = \frac{u}{\mathcal{U}} \qquad T_a^{\nu} = \frac{T^{\nu}}{\rho\nu\mathcal{U}d_0/\lambda_0} \\
N_a &= \frac{N}{\mathcal{P}d_0/\lambda_0} \qquad V_a^t = \frac{V^t}{\mathcal{V}^t} \qquad \tilde{V}_a = \frac{\tilde{V}}{\tilde{\mathcal{V}}}
\end{aligned}$$

With these assumptions, the nondimensional equations may be written as:

$$\begin{aligned}
\frac{\partial \zeta_a}{\partial t_a} + \frac{\partial}{\partial x_a}((\epsilon\zeta_a + d_a)u_a) &= 0 \qquad (5) \\
\frac{\partial}{\partial t_a}((\epsilon\zeta_a + d_a)u_a) + \epsilon\frac{\partial}{\partial x_a}\left((\epsilon\zeta_a + d_a)u_a^2\right) + (\epsilon\zeta_a + d_a)\frac{\partial \zeta_a}{\partial x_a} &= -\frac{1}{2}f_r\frac{\epsilon}{\mu^{1/2}}|u_a|u_a \\
+\frac{1}{Re}\frac{\partial T_a^{\nu}}{\partial x_a} + K_1\frac{\partial V_a^t}{\partial x_a} + K_2\frac{\partial \tilde{V}_a}{\partial x_a} &+ \mu N_a \qquad (6)
\end{aligned}$$

with five characteristic dimensionless parameters:

$$\epsilon = \frac{a_0}{d_0} = \frac{1}{2}\frac{H_0}{d_0} \qquad \mu = \frac{d_0^2}{\lambda_0^2} \qquad Re = \frac{\lambda_0 c_0}{\nu}$$
$$K_1 = \frac{\mathcal{V}^t}{\rho g d_0 a_0} \qquad K_2 = \frac{\tilde{\mathcal{V}}}{\rho g d_0 a_0}$$

The dimensionless number ϵ characterizes the non-linearity of the wave field. Laboratory observations of monochromatic waves on planar beaches (e.g. Bowen et al. (1968) or Svendsen et al. (1978)) and field measurements (e.g. Thornton and Guza (1982), Raubenheimer et al. (1996) or Sénéchal et al. (2001)) suggest that the heights H of broken waves in the ISZ are depth limited: $H = \gamma \bar{h}$ (where $\bar{h}$ is the time-average water depth), with γ weakly depending on μ, the beach slope β and the offshore wave steepness. The observed values of γ are about 0.6. From these observations we can estimate that in the ISZ the order of magnitude of $\epsilon = \frac{1}{2}\frac{H_0}{d_0} \simeq \gamma/2$ is about 0.3, which indicates that RWR dynamics is a moderately nonlinear process.

The non-dimensional parameter $\mu = d_0^2/\lambda_0^2$ characterizes non-hydrostatic and frequency dispersion effects. In the ISZ, μ is generally much smaller than 10^{-2}. Lin and Liu (1998), using a numerical model based on the Reynolds equations, showed that the pressure distribution under the spilling breaking wave is almost hydrostatic in RWR, with a maximum deviation from hydrostatic pressure of only 7%, which occurs in WF.

The dimensionless parameter $f_r \frac{\epsilon}{\mu^{1/2}}$ is generally much smaller than 1 in the ISZ, but its value increases shoreward and becomes of order 1 in the swash zone. Thus, the friction term must be retain in equation (6) due to its significant contribution in the swash zone.

In water waves of reasonable scale, the Reynolds number Re is much greater than 1 and the integrated viscous stress term can be neglected.

The dimensionless parameter K_1 characterizes the relative importance of the excess horizontal momentum flux due to turbulence compared to the depth averaged horizontal momentum flux. Several laboratory experiments on regular spilling breakers (e.g. Svendsen (1987) or Ting and Kirby (1996)) showed that the variation of turbulence intensity $\langle v_1'^2 \rangle^{1/2}$ over the depth is very small in RWR and that $\langle v_1'^2 \rangle^{1/2}$

varies nearly proportionally to $(g\bar{h})^{1/2}$: $\langle v_1'^2 \rangle^{1/2} = \alpha_1 (g\bar{h})^{1/2}$, with $\alpha_1 \sim 5.10^{-2}$. George et al. (1994) observed the same turbulent characteristics in natural surf zone, excepted that they found a smaller coefficient than in existing laboratory studies : $\alpha_1 \sim 10^{-2}$. From these observations we can estimate that $|V^t| \simeq \rho \langle v_1'^2 \rangle h \simeq \rho \alpha_1^2 g \bar{h} h$, which gives a characteristic scale $\mathcal{V}^t = \rho \alpha_1^2 g d_0^2$. Then, the dimensionless number $K_1 = \alpha_1^2/\epsilon$ ranges from about 10^{-3} to 10^{-2}. Consequently, in RWR the contribution of the depth integrated turbulent flux is small in equation (6).

The dimensionless parameter K_2 characterizes the relative importance of the excess horizontal momentum flux due to vertical non-uniformity of the velocity profile compared to the depth averaged horizontal momentum flux. Experiments by Cox (1995) and Ting and Kirby (1996) have shown that in RWR the ensemble-averaged horizontal velocity $\langle v_1 \rangle$ is nearly vertically uniform. This property is illustrated in figure 2 from velocity data measured in the ISZ by Cox (1995). These experiments were conducted in a wave flume with a beach slope of 1 : 35. The wave period T was 2.2 s and the wave height was selected to generate spilling breakers. Figure 2a shows the temporal variation of the nondimensional phase-averaged free surface elevation $\langle \zeta \rangle / a_0$ and figure 2b vertical variations of nondimensional phase-averaged horizontal velocity $\langle v_1 \rangle / \mathcal{U}$. We observe a strong vertical variation of $\langle v_1 \rangle / \mathcal{U}$ in the WF (figure 2b, $t_a = 2/6$), but a nearly vertically uniform horizontal velocity field in RWR. From Cox's data set corresponding to four different x locations in the ISZ, we have estimated that in RWR K_2 is about 10^{-3}. Consequently, inside RWR the contribution of the excess horizontal momentum flux due to vertical non-uniformity of the velocity profile is small in equation (6).

From this scaling analysis we have shown that in RWR the contributions of $\frac{\partial}{\partial x}\left(T^{\nu}\right)$, $\frac{\partial}{\partial x}\left(V\right)$ and N are small in equation (2). This explains why a model based on both, NSW equations (equations (3) and (4)) for regular or continuous parts of the wave field (RWR) and discontinuities satisfying appropriate shock conditions for thin wave fronts (WF), represents an appropriate tool for predicting periodic-wave transformation in the ISZ.

3 Periodic weak solutions to the NSW equations

In the first part of this section, we briefly recall the derivation of the NSW shock-wave solution (or weak NSW solution). The classical presentation (e.g. Stoker (1957) and Johnson (1997)) is extended by taking into account non-flat bottom and friction effects. In a second part, the shock-wave approach is applied to derive time-averaged equations for periodic broken waves. In particular, we proposed a new equation which gives the wave setup as a function of the broken-wave energy dissipation. In this section, we show that the NSW shock-wave model is a less restrictive approach than the classical bore model (see appendix A) which is generally used in coastal engineering.

3.1 Shock conditions and local dissipation

Our model associates the NSW equations with friction for the regular part of the wave field, and discontinuities for wave fronts. Resulting discontinuous solutions clearly do not satisfy the partial differential equations (equations (3) and (4)) in the classical sense, since the derivatives are not defined at discontinuities. We can, however, interpret the derivatives in the sense of distributions, using the mathematical concept of weak solutions (e.g. Whitham (1974) and Serre (1996)). To impose uniqueness of the solution it is necessary to derive other conditions to pick out the physically correct solution. These conditions are called mathematical entropy conditions by analogy with gas dynamics.

We return to the integral forms of the mass and momentum conservation laws, which still apply to discontinuous solutions. Let us consider a region made up of water lying between two vertical planes $x = x_a(t)$ and $x = x_b(t)$, such that, these planes contain always the same fluid particles. This assumption can be justified by the fact that in our study the vertical variability of the velocity field can be neglected ($K_2 \ll 1$). We suppose that there is a discontinuity at $x = x_s(t)$, between $x = x_a(t)$ and $x = x_b(t)$. The laws of conservation of mass and momentum are applied to the fluid domain $[x_a, x_b]$:

$$\begin{aligned} \frac{d}{dt}\left(\int_{x_a(t)}^{x_b(t)} \rho h \; dx\right) &= 0 \qquad (7) \\ \frac{d}{dt}\left(\int_{x_a(t)}^{x_b(t)} \rho h u \; dx\right) &= F_o \qquad (8) \end{aligned}$$

where $F_o = -\frac{1}{2}\rho g(h^2(x_b) - h^2(x_a)) + \int_{x_a}^{x_b} \rho g h \frac{\partial d}{\partial x} \; dx - \int_{x_a}^{x_b} \tau^b \; dx$ is the x-component of the sum of body and surface forces acting on the fluid domain. These conservation equations can be written

$$\int_{x_a}^{x_s} (\frac{\partial h}{\partial t} + \frac{\partial hu}{\partial x}) \; dx + \int_{x_s}^{x_b} (\frac{\partial h}{\partial t} + \frac{\partial hu}{\partial x}) \; dx + [hu] - c_b[h] = 0 \qquad (9)$$

$$\begin{aligned} \int_{x_a}^{x_s} (\frac{\partial hu}{\partial t} + \frac{\partial hu^2}{\partial x}) \; dx \;&+\; \int_{x_s}^{x_b} (\frac{\partial hu}{\partial t} + \frac{\partial hu^2}{\partial x}) \; dx + [hu^2] - c_b[hu] = \\ &-\; \int_{x_a}^{x_s} \frac{\partial}{\partial x}(\frac{1}{2}\rho g h^2) \; dx - \int_{x_s}^{x_b} \frac{\partial}{\partial x}(\frac{1}{2}\rho g h^2) \; dx - [\frac{1}{2}\rho g h^2] \\ &+\; \int_{x_a}^{x_b} \rho g h \frac{\partial d}{\partial x} \; dx - \int_{x_a}^{x_b} \tau^b \; dx \qquad (10) \end{aligned}$$

where the brackets [ ] indicate a jump in the quantity and c_b is the shock velocity defined by $c_b = \frac{dx_s}{dt}$.

The shock conditions are obtained by considering the limit case in which the length of the domain tends to zero, in such a way, that the discontinuity remains inside the domain. When we do so, we obtain the following shock conditions

$$-c_b[h] + [hu] \;=\; 0 \qquad (11)$$

$$-c_b[hu] + [hu^2 + \frac{1}{2}gh^2] \quad = \quad 0 \quad . \tag{12}$$

A conventional notation is to use subscript 1 and 2 for values ahead and behind the shock respectively (see figure 1b). So the shock conditions may also be written in the form

$$u_1 - c_b \quad = \quad \epsilon_s \left(\frac{gh_2}{2h_1}(h_2 + h_1)\right)^{\frac{1}{2}} \qquad (\epsilon_s = \pm 1) \tag{13}$$

$$u_2 - c_b \quad = \quad \epsilon_s \left(\frac{gh_1}{2h_2}(h_2 + h_1)\right)^{\frac{1}{2}} \tag{14}$$

Two solutions are possible, depending on the sign of ϵ_s, but only one physical solution makes sense. The non-uniqueness of solutions is due to the fact that some physical processes, such as turbulence, have been neglected in the WF. To derive the correct solution we need an entropy condition. In our problem, the entropy condition is based on the fact that the law of energy conservation is not verified across a shock, because the particle crossing the shock must lose energy.

The energy conservation principle states that

$$\frac{dE}{dt} = W \tag{15}$$

where $E = \int_{x_a}^{x_b} \mathcal{E}\ dx$ is the total energy, $\mathcal{E} = \frac{1}{2}\rho(hu^2 + g(\zeta^2 - d^2))$ is the energy density of a column of fluid, and W is the work due to surface stresses at the boundaries of the fluid domain, $W = -\frac{\rho g}{2}(u(x_b)h^2(x_b) - u(x_a)h^2(x_a)) - \int_{x_a}^{x_b} u\tau^b\ dx$. Let us define the rate of energy dissipation D_b due to the presence of shock by

$$D_b = -\frac{dE}{dt} + W$$

This expression can be written

$$D_b = -\int_{x_a}^{x_s} (\frac{\partial \mathcal{E}}{\partial t} + \frac{\partial \mathcal{F}}{\partial x})\ dx - \int_{x_s}^{x_b} (\frac{\partial \mathcal{E}}{\partial t} + \frac{\partial \mathcal{F}}{\partial x})\ dx - [\mathcal{F}] + c_b[\mathcal{E}] - D_f \tag{16}$$

where $\mathcal{F} = \rho h u \ (\frac{1}{2}u^2 + g\zeta)$ is the energy flux density and $D_f = \int_{x_a}^{x_b} \frac{1}{2}\rho f_r |u| u^2 \ dx$ is the energy dissipation due to bottom friction.

In continuous parts of the flow, using the mass and momentum conservation equations (3) and (4) we obtain

$$\frac{\partial \mathcal{E}}{\partial t} + \frac{\partial \mathcal{F}}{\partial x} = -\frac{1}{2}\rho f_r |u| u^2 \ , \tag{17}$$

hence,

$$D_b = 0.$$

The law of energy conservation is verified and energy dissipation is only due to bottom friction.

If a shock occurs at $x = x_s(t)$, equation (16) yields the relation

$$D_b = -[\mathcal{F}] + c_b[\mathcal{E}] \tag{18}$$

which can be written using the shock conditions (13) and (14)

$$D_b = -\epsilon_s \ \frac{\rho g}{4}\Big(\frac{g(h_2 + h_1)}{2h_1 h_2}\Big)^{\frac{1}{2}}(h_2 - h_1)^3 \ .$$

We see, therefore, that the law of energy conservation (equation (15)) does not hold across a shock. If we postulate that the particles crossing the shock must lose energy due to turbulent processes that we have neglected, then

$$D_b = -[\mathcal{F}] + c_b[\mathcal{E}] > 0 \tag{19}$$

and consequently

$$\epsilon_s = -1.$$

Inequality (19) is employed to weed out physically inadmissible weak solutions. The energy density $\mathcal{E}$ is the mathematical entropy of the NSW equations.

The entropy weak solution is then characterized by the shock conditions

$$u_1 - c_b = -\Big(\frac{gh_2}{2h_1}(h_2+h_1)\Big)^{\frac{1}{2}} \tag{20}$$

$$u_2 - c_b = -\Big(\frac{gh_1}{2h_2}(h_2+h_1)\Big)^{\frac{1}{2}} \tag{21}$$

and the shock dissipation, or the "broken-wave dissipation",

$$D_b = \frac{\rho g}{4}\Big(\frac{g(h_2+h_1)}{2h_1h_2}\Big)^{\frac{1}{2}}(h_2-h_1)^3 \tag{22}$$

or, equivalently

$$D_b = \frac{\rho g}{4}\frac{|Q_b|}{h_1h_2}(h_2-h_1)^3 \tag{23}$$

where $Q_b = h_1(u_1 - c_b) = h_2(u_2 - c_b)$ is the volume flux across the shock in the coordinate system moving with the broken-wave celerity c_b.

As we could expect, these equations coincide with the classical shock conditions (see Stoker (1957)) obtained without friction and bottom slope effects. Mathematically, the composite solution, composed of continuously differentiable parts satisfying equations (3) and (4), together with jump conditions (20) (21) as well as inequality (19), can be considered a weak entropy solution of equations (3) and (4).

Expression (22) is often used in the coastal-engineering literature, but generally it is introduced from an analogy between a ISZ broken-wave and an hydraulic jump (e.g. Le Méhauté (1962) or Battjes and Janssen (1978)). However, the hydraulic jump is a special case of shock wave where the energy dissipation remains constant over time. It is worthwhile to note that the broken-wave dissipation given by equation (22) can be applied to any shallow-water broken wave, even to non-saturated breakers (see figure 1), and not only to hydraulic jumps.

3.2 Time-averaged energy dissipation and wave setup

Prediction of time-averaged quantities such as mean broken-wave energy dissipation or wave setup represents an important issue of wave modelling in the surf zone. These quantities are generally evaluated from mean equations obtained by using a time average over the wave period of mass, momentum and energy equations (e.g. Phillips (1977)). In the framework of NSW weak solutions, contribution of shock wave has to be carefully estimated when time average of non-conservative equations, such as the energy equation, is performed.

In nearshore applications, the time-averaged energy equation for periodic broken waves is generally introduced in the context of the classical bore model (see Svendsen et al. (1978) and Appendix A). In this section, we derive the time-averaged energy equation in a more general context based on the NSW shock-wave solution. We consider periodic broken waves of period T and the time average operator is defined as $\overline{(.)} = \frac{1}{T}\int_t^{t+T} (.)\, d\tau$. To derive the mean energy equation we develop the expression of the mean energy flux gradient $\frac{\partial \bar{\mathcal{F}}}{\partial x}$

$$
\begin{aligned}
T\frac{\partial \bar{\mathcal{F}}}{\partial x} &= \frac{\partial}{\partial x}\left(\int_t^{t+T} \mathcal{F}\, d\tau\right) = \frac{\partial}{\partial x}\left(\int_t^{t_s^-} \mathcal{F}\, d\tau\right) + \frac{\partial}{\partial x}\left(\int_{t_s^+}^{t+T} \mathcal{F}\, d\tau\right) \\
&= \int_t^{t_s^-} \frac{\partial \mathcal{F}}{\partial x}\, d\tau + \frac{dt_s}{dx}\mathcal{F}(t_s^-) + \int_{t_s^+}^{t+T} \frac{\partial \mathcal{F}}{\partial x}\, d\tau - \frac{dt_s}{dx}\mathcal{F}(t_s^+)\ .
\end{aligned}
$$

where $t_s(x)$ is the time at which the shock is located in x. Using equation (17) we obtain

$$
\begin{aligned}
T\frac{\partial \bar{\mathcal{F}}}{\partial x} &= -\int_t^{t_s^-} \frac{\partial \mathcal{E}}{\partial t}\, d\tau - \int_{t_s^+}^{t+T} \frac{\partial \mathcal{E}}{\partial t}\, d\tau - \int_t^{t+T} \frac{1}{2}\rho f_r |u| u^2\, d\tau + \frac{1}{c_b}[\mathcal{F}] \\
&= \frac{1}{c_b}([\mathcal{F}] - c_b[\mathcal{E}]) - \int_t^{t+T} \frac{1}{2}\rho f_r |u| u^2\, d\tau
\end{aligned}
$$

and finally

$$\frac{\partial \bar{\mathcal{F}}}{\partial x} = -D_{b_m} - D_{f_m} \ , \tag{24}$$

where $D_{b_m} = D_b/(c_b T)$ is the mean broken-wave dissipation and $D_{f_m} = \frac{1}{2}\rho f_r \overline{|u|u^2}$ is the mean bottom friction dissipation. Using equations (22) and (23), D_{bm} writes

$$D_{b_m} = \frac{\rho g}{4 c_b T}\Big(\frac{g(h_2+h_1)}{2h_1h_2}\Big)^{\frac{1}{2}}(h_2-h_1)^3 \tag{25}$$

or, equivalently

$$D_{b_m} = \frac{\rho g}{4 c_b T}\frac{|Q_b|}{h_1 h_2}(h_2-h_1)^3 \ . \tag{26}$$

In case of saturated breakers ($h_2 - h_1 = H$), the dissipation expression (25) reduces to the classical bore model (equation (43) in appendix A) when the broken-wave celerity c_b is estimated using a quasi-constant wave-form assumption (equation (42) in appendix A). We will show in section 5 that this assumption leads to a c_b-model which underestimates the actual broken-wave celerity.

It is worthwhile to note that the mean energy dissipation equations (25) and (26) have been established in a less restrictive context than those of the classical bore model (see appendix A). In particular, we do not need to assume a quasi-constant wave form and we can also consider non-saturated breakers ($h_2 - h_1 < H$).

Now a new time-averaged equation to determine the wave setup $\bar{\zeta}$ is derived from the non-conservative momentum equation

$$\frac{\partial u}{\partial t} + \frac{\partial}{\partial x}\left(\frac{1}{2}u^2 + g\zeta\right) = -\frac{1}{2}\frac{f_r|u|u}{h} \ . \tag{27}$$

To derive the setup equation we develop the expression of the gradient $\frac{\partial \bar{\mathcal{M}}}{\partial x}$, where $\mathcal{M} = \frac{1}{2}u^2 + g\zeta$,

$$T\frac{\partial \bar{\mathcal{M}}}{\partial x} \;=\; \frac{\partial}{\partial x}\left(\int_t^{t_s^-} \mathcal{M}\, d\tau\right) + \frac{\partial}{\partial x}\left(\int_{t_s^+}^{t+T} \mathcal{M}\, d\tau\right)$$

$$= \int_t^{t_s^-} \frac{\partial \mathcal{M}}{\partial x}\, d\tau + \frac{dt_s}{dx}\mathcal{M}(t_s^-) + \int_{t_s^+}^{t+T} \frac{\partial \mathcal{M}}{\partial x}\, d\tau - \frac{dt_s}{dx}\mathcal{M}(t_s^+)$$

Using equation (27) we obtain

$$\begin{aligned} T\frac{\partial \bar{\mathcal{M}}}{\partial x} &= -\int_t^{t_s^-} \frac{\partial u}{\partial t}\, d\tau - \int_{t_s^+}^{t+T} \frac{\partial u}{\partial t}\, d\tau - \int_t^{t+T} \frac{1}{2}\frac{f_r|u|u}{h}\, d\tau + \frac{1}{c_b}[\mathcal{M}] \\ &= \frac{1}{c_b}([\mathcal{M}] - c_b[u]) - \int_t^{t+T} \frac{1}{2}\frac{f_r|u|u}{h}\, d\tau \end{aligned}$$

The expression $[\mathcal{M}] - c_b[u]$ is computed using shock conditions (20) and (21)

$$[\mathcal{M}] - c_b[u] = \frac{g}{4}\frac{(h_2 - h_1)^3}{h_2 h_1} = \frac{D_b}{\rho|Q_b|} \ .$$

From this expression we find

$$\frac{\partial \bar{\mathcal{M}}}{\partial x} = \frac{D_{bm}}{\rho|Q_b|} - \frac{1}{2} f_r \overline{|u|u/h}$$

and finally

$$\frac{\partial \bar{\zeta}}{\partial x} = \frac{D_{bm}}{\rho g|Q_b|} - \frac{1}{g}\frac{\partial}{\partial x}\left(\overline{\frac{1}{2}u^2}\right) - \frac{1}{2g} f_r \overline{|u|u/h} \ . \tag{28}$$

In this equation the friction term can be generally neglected. The main contribution for wave setup is due to the first term on the right-hand side of equation (28), $\frac{D_{bm}}{\rho g|Q_b|}$, which is related to the broken-wave energy dissipation. This term can also be written

$$\frac{D_{bm}}{\rho g|Q_b|} = \frac{1}{4 c_b T}\frac{(h_2 - h_1)^3}{h_1 h_2} \ .$$

To our knowledge, it is the first study which explicitely shows, from a non-linear theory, that broken-wave energy dissipation D_{bm} acts as a wave driving term in the mean momentum equation. However, previous studies (Longuet-Higgins (1973) and Dingemans at al. (1987)) based on the linear wave theory already showed that the wave driving force in the mean momentum equation can be written in function of

D_{bm}. We will show in section 5 that equation (28) can represent an alternative to classical time-averaged methods (e.g. Longuet-Higgins and Stewart (1964) and Mei (1989)) for computing wave setup in the surf zone.

4 A one-way broken-wave model

The motion of a single bore propagating into water at rest on a beach has been studied for a long time. One-way analytical solutions of this phenomenon were first given by Whitham (1958) and Ho and Meyer (1962), and numerical simulations were performed by Keller et al. (1960) and Hibberd and Peregrine (1979). On the other hand, only few studies have been devoted to the propagation of periodic broken waves on a gently sloping beach. This is mainly due to the fact that shock-wave conditions are more complex for periodic broken waves (velocity ahead the wave front, u_1, is negative), than for a single bore which propagates into quiescent water ($u_1 = 0$).

In this section, we present a simplified one-way version of the NSW shock-wave model, which applies to the transformation of non-reflective periodic broken waves on gently sloping beaches. Even if numerical solutions of the complete NSW model can be now easily computed, a simplified one-way approach is useful to provide breaking-wave parameterizations in both, time-averaged wave models (e.g. Svendsen et al. (2003)) and time-dependent Boussinesq-type models (e.g. Madsen et al. (1997)). In particular, the estimation of the broken-wave celerity from a one-way approach is a key point of these parameterizations (Bonneton (2004)).

We first consider the case of wave propagation on a horizontal bottom. Such a situation represents an interesting limiting case of wave propagation on a gently sloping beach, even if in this case dispersive mechanisms actually play a significant role. If the still water depth is constant, $d = d_0$, and the friction term is discarded, the hyperbolic system of equations (3) and (4) may be expressed by two characteristic equations,

$$\left\{\frac{\partial}{\partial t} + (u \pm c)\frac{\partial}{\partial x}\right\}(u \pm 2c) = 0 \tag{29}$$

where $c(h) = (gh)^{\frac{1}{2}}$. The Riemann invariants $\alpha^{\pm} = u \pm 2c$ are constant along characteristic curves $C^{\pm}$ defined by $\frac{dx}{dt} = u \pm c$.

The weak solution theory becomes particularly simple in the case of problems in which the wave field has one of the Riemann invariants constant throughout. A wave solution corresponding to such a situation is called a "simple wave" (see Stoker (1957)). For instance, if a wave is propagating in the positive x-direction into water of constant depth d_0 and constant velocity u_0 , α^- is constant and given by

$$\alpha^- = u - 2c = u_0 - 2c_0 \tag{30}$$

with $c_0 = (gd_0)^{\frac{1}{2}}$. Consequently, the two NSW equations reduce to a one-way equation which is either, the mass conservation equation

$$\frac{\partial h}{\partial t} + \frac{\partial q(h)}{\partial x} = 0 \tag{31}$$

or the momentum conservation equation

$$\frac{\partial q(h)}{\partial t} + \frac{\partial}{\partial x}\left(q(h)^2/h + 0.5gh^2\right) = 0 \tag{32}$$

where $q(h) = hu = h(u_0 - 2c_0 + 2c(h))$. These two equations are equivalent provided that the wave solution is continuous. However, when a shock is involved, this equivalency no longer hold, because there is a jump in α^- quantity at the shock. This jump, $[\alpha^-]$, can be obtained by subtracting equation (21) from equation (20). We find

$$[\alpha^-] = -2\left(g(h_1 + h_2)/2\right)^{\frac{1}{2}}\left(\frac{\epsilon}{(1-\epsilon^2)^{1/2}} - (1+\epsilon)^{1/2} + (1-\epsilon)^{1/2}\right) \tag{33}$$

where $\epsilon = (h_2 - h_1)/(h_2 + h_1)$ is the shock strength. Bonneton (2001) has shown that for shocks of moderate strength, such as ISZ-shocks where $\epsilon \sim \gamma/2 \sim 0.3$ (see section 2), neglecting changes in the Riemann invariant α^- constitutes a reasonable approximation, and so equation 30 can be applied even at a shock.

This approximation allows the one-way equation (31) to be retained and combined with the shock condition, $-c_{b_s}[h] + [q(h)] = 0$, which yields the relation

$$c_{b_s} = u_0 - 2c_0 + 2g^{\frac{1}{2}} \frac{h_2^{3/2} - h_1^{3/2}}{h_2 - h_1} \ , \tag{34}$$

where c_{b_s} is the one-way shock-wave celerity. The energy dissipation D_{b_s} is given by $D_{b_s} = -[\mathcal{F}] + c_{b_s}[\mathcal{E}]$, which leads to

$$D_{b_s} = \frac{\rho}{g}(c_2 - c_1)^3 \left(c_2^2 + 3c_1c_2 + c_1^2 + (u_0 - 2c_0)\frac{(c_2^2 + 4c_1c_2 + c_1^2)}{2(c_2 + c_1)} \right) \ , \tag{35}$$

with $c_1 = c(h_1)$ and $c_2 = c(h_2)$. Celerity c_{b_s} and dissipation D_{b_s} are approximations of the exact shock celerity c_b and dissipation D_b. Figure 3 presents the relative errors $(c_b - c_{b_s})/c_{b_s}$ and $(D_b - D_{b_s})/D_{b_s}$ in function of the shock strength ϵ, assuming that $\frac{(h_2+h_1)/2}{d_0} \sim 1$ and $u_0 = 0$. This figure shows that, even if c_{b_s} and D_{b_s} are smaller than c_b and D_b, they represent good approximations when the shock is either weak, or of moderate strength, as in the case of ISZ broken waves.

Figure 4 presents the time evolution of the energy dissipation D_{b_s} of an initial sine wave propagating on a flat bottom. Energy dissipation starts when the shock forms at $t = t_s$, increases up to $t \simeq 1.6t_s$ and progressively decreases. This evolution, which is due to continuous broken-wave distortion, is definitely different from those of a hydraulic jump. Indeed, the hydraulic jump reaches immediately its full strength and the energy dissipation remains constant over time.

Let us consider now in more detail the energy dissipation mechanisms involved in the weak-solution theory. One useful technique for determining weak solutions of the one-way equation (31) is to apply the method of characteristics and then eliminate the multi-valued parts by inserting shocks. To find the appropriate location of the shock, Whitham (1974) proposed an ingenious method called "the equal area rule". The shock is located so that the regions cut off on either side have equal areas, as in figure 5. This is a consequence of mass conservation: the integral of the discontinuous weak solution must be the same as the area under the multi-valued solution, since both are subject to the same conservation law. It is important to emphasize again that the energy of the weak solution is not conserved in the presence of shocks. Figure 5 clearly shows that the mass redistribution at the shock induces a decrease of the potential energy, in accordance with the actual physical wave breaking process. Then, the equal area rule gives us a better understanding of the energy dissipation mechanisms involved in the weak-solution theory. If the present discussion of dissipation processes remains qualitative, we will show in section 5 that there is also a good quantitative agreement between theoretical and measured broken-wave energy dissipation.

Let us consider now a more realistic case where periodic broken waves propagate over a sloping beach. In that case, the onshore mass transport associated with waves propagating towards the shore is balanced by an offshore mean flow $\bar{u}$. Moreover, as described in section 3.2, broken-wave dissipation induced a wave setup $\bar{\zeta}$. So, the periodic broken waves propagate into a water depth $\bar{h}$ with a mean current $\bar{u}$. We can consider that for a gently sloping beach wave reflexion is negligible.

Indeed, Peregrine (1967) theoretically showed that for periodic non-broken waves on a gently sloping beach, wave reflexion is very small. Moreover, in the ISZ the wave energy decreases shoreward due to wave breaking and then wave reflexion at the shoreline is very small. So, for a gently sloping beach we can estimate that locally α^- is constant and can be evaluated using equation (30), $\alpha^- = u - 2c \simeq \bar{u} - 2c_m$, with $c_m = (g\bar{h})^{\frac{1}{2}}$. Considering that $u - 2c$ is a slow-varying function of x, which is not dependent on time, we obtain the following relation:

$$u - 2c = \bar{u} - 2\bar{c} \; . \tag{36}$$

With this relation, the NSW equations can be reduced to a one-way equation:

$$\frac{\partial h}{\partial t} + \frac{\partial}{\partial x}\left\{h\left(\bar{u} - 2\bar{c} + 2(gh)^{1/2}\right)\right\} = 0 \tag{37}$$

with the shock condition, $-c_{b_s}[h] + [q(h)] = 0$, which yields the relation

$$c_{b_s} = \bar{u} - 2\bar{c} + 2g^{\frac{1}{2}}\frac{h_2^{3/2} - h_1^{3/2}}{h_2 - h_1} \; . \tag{38}$$

We will show in the next section, that this one-way model gives good results for describing the non-linear transformation of periodic broken waves in the ISZ.

5 Comparisons between model results and laboratory data

In this section, we will assess the ability of both the complete NSW model and the simplified one-way model to predict the transformation of periodic ISZ broken waves. We present comparisons between numerical solutions and spilling breaking experiments.

The main set of comparisons is based on an experiment performed by Cox (1995). This experiment was carried out in a wave flume 33 m long, 0.6 m wide and 1.5 m deep. Waves were generated on a horizontal bottom at a depth of 0.40 m, shoaled, and broke on a 1:35 planar slope. The wave height at the wavemaker was $H_w = 0.115$ m and the wave period $T = 2.2$ s. Measurements of surface elevation and velocity were taken at four locations inside the ISZ (see figure 6). The velocities were measured with a two-component laser Doppler velocimeter (LDV).

NSW and one-way equations are solved with the same shock-capturing numerical method: a TVD Mac Cormack scheme. The implementation of this method for solving the NSW equations is presented in appendix B. The seaward boundary condition of the two models is given by time series of water depth measured at the first location L1. The computational domain was discretized by 200 nodes using a grid spacing of $\Delta x = 0.04$ m, and the models were run with a time step $\Delta t = 0.01$ s. The spatial and time steps corresponded respectively to $\Delta x = \lambda_0/72$ and $\Delta t = T/220$, where λ_0 is the wavelength at the seaward boundary L1.

5.1 NSW shock-wave model

The initial condition of no wave motion (still water) leads to a transient period of 200 s, which is eliminated from time series presented hereafter. Previous numerical studies by Kobayashi et al. (1987) and Cox (1995) have shown that ISZ predictions were not very sensitive to the value of the friction coefficient f_r, when $0.01 \leq f_r \leq 0.05$. In the subsequent computations we used a fixed coefficient $f_r = 0.015$.

Figure 7 shows computed and measured time series of surface elevation at different locations inside the ISZ. The NSW model reproduces the nonlinear wave distortion and gives a good prediction of the wave height decay. The evolution towards the sawtooth shape is accurately computed by the model. Previous studies, using NSW models (Kobayashi et al. (1989), Tega and Kobayashi (2002)) or Boussinesq models (Madsen et al. (1997) and Ozanne et al. (2000)), showed numerical oscillations at the rear of wave fronts. We can see in figure 7 that our shock-capturing method prevents such numerical oscillations. The good phase agreement between computed and measured time series shows that the shock velocity c_b, given by the shock conditions (equations (20) and (21)), is a good estimate of the wave front velocity.

To emphasize this point we present in figure 8 a comparison between experimental wave front positions and a wave front trajectory computed by the NSW model. In addition, we plot in this figure trajectories computed from two other wave front celerity expressions. The first one, $c_{b1} = \Big((gh_1h_2(h_1+h_2))/(2\bar{h}^2)\Big)^{1/2}$, corresponds to the classical bore model (see appendix A). The second one, $c_{b2} = 1.3(gd)^{1/2}$, is an empirical expression which is usually applied to estimate wave front celerity (or roller celerity) in Boussinesq models (Schäffer et al. (1993)). Figure 8 shows a very good agreement between measured wave front positions and NSW model results. We observe that trajectories computed from c_{b1} and c_{b2} are close to the measured trajectories. However, as already noticed by Bonneton (2004), the expression c_{b2} slightly overestimates the wave front celerity and can not be applied in the swash zone, and c_{b1} slightly underestimates the wave front celerity. The ability of the NSW weak solution to predict the wave front celerity is not limited to regular waves. Bonneton et al. (2005) have shown that the NSW model also gives an accurate prediction for the celerity of irregular waves propagating over gently sloping beaches.

Figure 9 shows the cross-shore variations of the minimum and maximum values of wave elevation, ζ_{min} and ζ_{max}. We observe that computed ζ_{min} and ζ_{max} are in close agreement with measurements. Model-data comparisons from another spilling breaking experiment, performed by Ting and Kirby (1996), are presented in figure 10. This experiment is similar to Cox's experiment, with $\beta = 1/35$, $T = 2$ s and $H_w = 0.125$ m, but the ζ-measurement spatial density is higher. Figure 10 confirms the ability of the NSW model to predict ζ_{min} and ζ_{max} cross-shore variations, and then the wave height decay in the ISZ.

To go further in analyzing the predictive capability of the NSW model, the results are compared with the phase-averaged measured horizontal velocities $\langle v_1 \rangle$. The measurements are limited to the regions away from the crest because with the LDV technique it is not possible to measure velocities in the highly aerated region near the front of the breaker. Figure 11 shows the vertical variations of $\langle v_1 \rangle$, measured at L3 for times $t = t_*$, $t = t_* + T/6$, $t = t_* + 2T/6$, $t = t_* + 3T/6$, $t = t_* + 4T/6$ and $t = t_* + 5T/6$, where t_* is the time at which the zero-upcrossing of the surface elevation occurs. The solid line represents the vertical average of these velocity data, $u_m = \frac{1}{\zeta_m + d}\int_{-d}^{\zeta_m} \langle v_1 \rangle \; dz$, where ζ_m is the highest measurement elevation. As already noticed in section 2, the wave field in the regular wave region RWR is characterized by a nearly vertically uniform horizontal velocity (see figures 11a,b,e,f). In RWR, we observe that the computed depth-averaged velocity u is a good estimate of $\langle v_1 \rangle$. Conversely, the wave front WF is characterized by a strong vertical variation of $\langle v_1 \rangle$ (see figure 11c). In this zone, u is not representative of the velocity $\langle v_1 \rangle$ below $z = \zeta_m$ and is much greater than u_m.

Figure 12 presents the temporal variations of computed and measured depth-averaged velocities at locations L1, L2, L3 and L4. This figure shows that, in the RWR and particularly in the wave trough, u is a good estimate of u_m. Conversely, we observe that in the WF, u is much greater than u_m. This observation does not necessary challenge NSW weak-solutions. Indeed, we do not compare exactly the same quantities, since u_m is integrated between $z = -d$ and $z = \zeta_m$ and u is integrated over the whole depth. Moreover, we know from Particle Image Velocimetry (PIV) observations (e.g. Govender et al. (2002)), that $\langle v_1 \rangle$ is much greater in the front part of the wave crest ($z > \zeta_m$) than in the lower part. An accurate PIV determination of the depth-averaged velocity (over the whole depth), would be very useful to make clear the validity limits of NSW weak-solutions in the ISZ.

For regular broken waves propagating over a low-slope beach, such as those experimentally studied by Cox (1995) and Ting and Kirby (1996), wave reflexion is small. Figure 13 presents the computed Riemann invariant $\alpha^- = u - 2c$, at a given time, as a function of x. This figure shows that α^- is approximately equal to $\bar{u} - 2\bar{c}$, excepted close to the shoreline. In accordance with the simple-wave solution presented in section 4, we observe small jumps in α^- at shocks (see equation (33)). Nevertheless, $\bar{u} - 2\bar{c}$ is a good estimate of α^- in the ISZ. This result confirms the validity of the main hypothesis on which our one-way model is based.

5.2 One-way shock-wave model

One-way solutions are determined from an iterative method, starting with $\bar{h} = d(x)$ and $\bar{u} = 0$ at the first iteration. Wave elevation fluctuations, $\tilde{\zeta} = h - \bar{h}$, and wave velocity fluctuations, $\tilde{u} = u - \bar{u}$, are computed from equations (37) and (38). Then, a new estimate of $\bar{u}$ is calculated from the time-averaged mass conservation equation

$$\bar{u} = -\frac{1}{\bar{h}}\overline{\tilde{\zeta}\tilde{u}}$$

and $\bar{h} = \bar{\zeta} + d$ is given by the new setup expression (see section 4) neglecting the friction term

$$\frac{\partial\bar{\zeta}}{\partial x} = \frac{1}{4c_b T}\frac{(h_2 - h_1)^3}{h_1 h_2} - \frac{1}{g}\frac{\partial}{\partial x}\left(\overline{\frac{1}{2}u^2}\right) \ , \tag{39}$$

or alternatively is given by the classical setup model (see Longuet-Higgins and Stewart (1964) or Mei (1989))

$$\frac{\partial\bar{\zeta}}{\partial x} = -\frac{1}{\rho g\bar{h}}\frac{\partial\tilde{S}}{\partial x} \ , \tag{40}$$

where $\tilde{S} = \rho(\bar{h}\overline{\tilde{u}^2} + \frac{1}{2}g\overline{\tilde{\zeta}^2} + \overline{\tilde{\zeta}\tilde{u}^2} - \overline{\tilde{\zeta}\tilde{u}}^2/\bar{h})$ is the radiation stress in shallow water. The iterative method requires about five iterations to converge to the solution.

Comparisons between one-way results and measurements by Cox (1995), figure 14, and Ting and Kirby (1996), figure 15, are presented. In these two figures, we can see that the one-way shock-wave model gives a good prediction of the wave elevation field, and in particular the wave height decay and the mean setup. Contrary to the NSW model, the one-way model slightly underestimates ζ_{min}. However, we observe in figures 14 and 15 that computed ζ_{min} and ζ_{max} are globally in agreement with measurements.

Figures 14 and 15 also show that one-way solutions propagate slightly slower than NSW solutions. This observation is coherent with the simple-wave hypotheses which lead to a shock celerity c_{b_s} slightly smaller than the exact NSW celerity c_b (see figure 3). However, figure 16 shows that trajectories computed from the one-way model are closed to the measured trajectories. In particular, the one-way model gives better results than the classical bore model. Bonneton (2004) has presented a more detailed analysis of ISZ broken-wave kinematics and proposed a c_b-expression slightly more accurate than equation (38).

5.3 Energy dissipation and wave setup

We discuss now the ability of NSW and one-way shock-wave solutions to predict time-averaged wave quantities such as potential energy, $E_p = \frac{1}{2}\rho g\overline{(\zeta - \bar{\zeta})^2}$, and wave setup $\bar{\zeta}$.

Figure 17 presents the cross-shore variation of the potential energy E_p. This figure shows that NSW and one-way models give good predictions of the shoreward spatial decrease of E_p. These results confirm a previous work, by Bonneton (2001)), which showed that the mean energy dissipation predicted by the shock-wave concept, D_{b_m}, was in agreement with experimental measurements. Previous studies by Svendsen et al. (1978) and Stive (1984), about ISZ energy dissipation, led to different conclusion. Analyzing the contribution of the various terms in the energy equation (24), these authors showed that the actual energy dissipation was substantially larger than the shock-wave dissipation D_{b_m}. However, the experimental estimation of the energy flux $\bar{\mathcal{F}}$ required detailed velocity information in the broken-wave crest, which were not available. The energy flux $\bar{\mathcal{F}}$ was estimated from velocity extrapolation which reduced the accuracy of the analysis. Moreover, D_{b_m} was estimated using the classical bore model, which gives only an approximation of the mean shock-wave dissipation (see appendix A). Conversely, results presented in this paper (figures 9, 10, 14, 15 and 17), as well as previous numerical results by Kobayashi et al. (1989), Cox (1995) and Bonneton et al. (2000, 2001, 2005), indicate that the local shock-wave energy dissipation D_b (equation (25)), or its one-way formulation D_{b_s} (equation (35)), represent good estimates of the actual energy dissipation.

Figure 18 presents the measured and computed variations of the time-averaged free surface elevation $\bar{\zeta}$, for a third spilling breaking experiment, performed by Buhr-Hansen and Svendsen (1979). We observe in the three figures 9, 10 and 18 that the setup $\bar{\zeta}$ is accurately predicted by the NSW model. This shows that the NSW weak solution represents an appropriate model for describing the ISZ setup.

As shown in figures 14, 15 and 19, the wave setup is also well predicted by the one-way shock-wave model. Figure 19 shows that the new setup equation (equation (39)) gives similar results than the classical setup equation (equation (40)). The new setup equation, which directly relies $\frac{\partial \bar{\zeta}}{\partial x}$ and shock characteristics (h_1, h_2 and c_b), can represent an useful alternative to the implicit classical setup formulation.

6 Conclusion

In this paper, we have presented a detailed analysis of the approximations involved in the time-dependent NSW shock-wave model. This model is based on the theory of weak solutions for conservative equations, which allows to predict global wave evolution without a detailed description of small-scale processes located at wave fronts. We have extended the classical presentation of NSW weak solutions (Stoker (1957)), by taking into account non-flat bottom and friction effects.

This shock-wave theory allows to derive time-averaged equations, such as the energy equation, in a more general context than the classical bore model (Svendsen et al. (1978)) generally used in coastal engineering. In particular, we have obtained, from time-averaging of the non-conservative momentum equation, a new equation (equation 28) to compute ISZ wave setup as a function of the energy dissipation.

We have also derived a new one-way shock-wave model (equations 37 and 38), which applies to the transformation of non-reflective periodic broken waves on gently sloping beaches. Even if numerical solutions of the complete NSW model can be easily computed, our simplified one-way approach is useful to provide breaking-wave parameterizations (in particular broken-wave celerity expression) in both time-averaged wave models and time-dependent Boussinesq-type models.

A detailed comparison with spilling wave-breaking experiments, has shown that both NSW and one-way shock-wave solutions compare very well with experimental data. Both models reproduce the nonlinear wave distortion leading to the sawtooth shape, and gives a good prediction of broken-wave celerity c_b, wave height decay and time-averaged quantities such as wave setup.

These results show that NSW weak solutions represent an appropriate theory for describing both time-varying and time-averaged quantities in the ISZ. Up to now, for ISZ time-averaged applications, NSW shock-wave theory was mainly used in a restricted context based on the classical bore model and the analogy between ISZ broken waves and hydraulic jumps (e.g. Le Méhauté (1962), Battjes and Janssen (1978) or Svendsen et al. (1978, 2003)). It is worthwhile to note that NSW shock-wave solutions can be applied to any ISZ broken wave and not only to hydraulic jumps. Contrary to previous studies by Svendsen et al. (1978) and Stive (1984), our results indicate that theoretical dissipation D_b (equation (22)) is a good estimate of the actual energy dissipation. To solve this controversy, and more generally to make clear validity limits of NSW weak-solutions, accurate PIV measurements in ISZ-wave fronts would be very useful.

Acknowledgment

This work was financially supported by the PATOM program (Programme ATmosphère Océan à Multi-échelle). We wish to thank Daniel Cox, Francis C.K. Ting and Luc Hamm (see Peronnard and Hamm (1995)) for providing the experimental data.

A The classical bore model

In most of time-averaged surf zone models, broken-wave celerity and energy dissipation are estimated from the classical bore model. This model, initially introduced by Le Méhauté (1962), is based on the analogy between a breaking wave and an hydraulic jump (see figure 20). In this appendix we briefly recall the main hypotheses of this model (see also Battjes (1978) and Svendsen et al. (1978, 2003)).

The classical bore model relies on two sets of approximations. The first one corresponds to the NSW hypotheses discussed in section 2 :

- A1: both vertical non-uniformity of the horizontal velocity and non-hydrostatic effects are negligible ($K_2 \ll 1$ and $\mu \ll 1$).

The second set of approximations stems from the analogy between broken waves and hydraulic jumps, illustrated in figure 20:

- A2: the bottom is considered as a locally horizontal bottom
- A3: the wave has a quasi-constant form
- A4: breaking waves are considered as saturated breakers (i.e. $H = h_2 - h_1$)

From mass and momentum conservation equations and using all the previous approximations it is straightforward to show that the volume flux in the reference frame moving at c_b, $Q = h(u - c_b)$, is spatially constant and given by

$$Q = -\Big(\frac{g h_1 h_2 (h_2 + h_1)}{2}\Big)^{\frac{1}{2}} \tag{41}$$

and that the local dissipation D_b writes

$$D_b = \frac{\rho g}{4} \frac{|Q|}{h_1 h_2} H^3 \ .$$

For a periodic wave field the total mean volume flux, $\overline{hu} = \bar{Q} + c_b\bar{h}$, is equal to zero. Since we assume that the wave has a quasi-constant form (A3 approximation), $\bar{Q} = Q$ and then

$$Q = -c_b\bar{h}.$$

Combining this expression with Eq. (41) we find the classical bore model for the broken-wave celerity

$$c_b = \Big(\frac{gh_1h_2(h_1+h_2)}{2\bar{h}^2}\Big)^{\frac{1}{2}}, \tag{42}$$

and for the mean energy dissipation $D_{bm} = D_b/(c_bT)$

$$D_{bm} = \frac{\rho g}{4T}\frac{\bar{h}}{h_1h_2}H^3\ , \tag{43}$$

where T is the wave period.

Most of time-averaged surf zone models are based on Equations (42) and (43) (e.g. Svendsen et al. (1978, 1984, 2003) or Stive (1984)), or on a simplified version of these equations (e.g. Battjes and Janssen (1978) or Thornton and Guza (1983)), with a linear estimate of the celerity, $c_b = (g\bar{h})^{\frac{1}{2}}$, and a mean dissipation given by

$$D_{bm} = \frac{\rho g}{4T}\frac{H^3}{\bar{h}}\ . \tag{44}$$

It is important to note that the classical bore model is associated with three approximations (A2, A3 and A4) which are not required in the NSW shock-wave approach. Equation (42) corresponds to an approximation of the broken-wave celerity c_b and then equation (43) is an approximation of the exact energy dissipation expression given by equation (25).

B Numerical scheme

First numerical simulations of broken-wave propagation on a beach (Hibberd and Peregrine (1979) and Kobayashi et al. (1989)) were based on the Lax-Wendroff scheme. This explicit finite-difference scheme, second-order accurate in space and time, has been successfully applied to solve numerous problems in gas dynamics. However, in the presence of fronts, the dispersive properties of this scheme introduce spurious numerical oscillations. Some dissipation is needed to give nonoscillatory shocks and to ensure that the numerical solution converges to the entropy weak solution. The most simple way to do this is to add an additional "artificial viscosity" term (e.g. Hibberd and Peregrine (1979) and Kobayashi et al. (1989)). The difficulty with this empirical approach is that it is hard to determine an appropriate "artificial viscosity" that introduces just enough dissipation to prevent numerical oscillations without causing unnecessary smearing. An alternative to this method is to use a TVD (total variation diminishing) flux limiter scheme, which represents a rational method for the determination of artificial dissipation terms (see LeVeque (1992)).

Following this approach, we have chosen a method based on a MacCormack scheme with a TVD flux limiter, which has been initially developed by Yee (1987) for solving the Navier Stokes compressible equations. The same method has been also implemented with success by Garcia-Navarro et al. (1992) to solve NSW equations for flood processes and hydraulic problems.

A brief presentation of the main steps of the numerical method is given here, but a complete description of the model can be found in Vincent et al. (2001). NSW equations can be expressed in vectorial form as:

$$\frac{\partial \mathbf{q}}{\partial t} + \frac{\partial \mathbf{F}}{\partial x} = \mathbf{S} \tag{45}$$

$$\mathbf{q} = \begin{pmatrix} h \\ hu \end{pmatrix}, \mathbf{F} = \begin{pmatrix} hu \\ hu^2 + \frac{1}{2}gh^2 \end{pmatrix}, \mathbf{S} = \begin{pmatrix} 0 \\ gh\frac{\partial d}{\partial x} - \frac{1}{2}f_r|u|u \end{pmatrix}.$$

Let $\mathbf{q}_i^n$ be the numerical solution of equation (45) at $x = i\Delta x$ and $t = n\Delta t$, with Δx the spatial mesh size and Δt the time step. The TVD MacCormack scheme can be expressed in three steps:

(a) predictor step

$$\mathbf{q}_i^1 = \mathbf{q}_i^n - \frac{\Delta t}{\Delta x}(\mathbf{F}_{i+1}^n - \mathbf{F}_i^n) + \Delta t \mathbf{S}_i^n$$

(b) corrector step

$$\mathbf{q}_i^2 = \frac{1}{2}\left(\mathbf{q}_i^1 + \mathbf{q}_i^n - \frac{\Delta t}{\Delta x}(\mathbf{F}_i^1 - \mathbf{F}_{i-1}^1) + \Delta t \mathbf{S}_i^1\right)$$

(c) TVD step

$$\mathbf{q}_i^{n+1} = \mathbf{q}_i^2 + \frac{\Delta t}{2\Delta x}(R_{i+\frac{1}{2}}^n \mathbf{\Phi}_{i+\frac{1}{2}}^n - R_{i-\frac{1}{2}}^n \mathbf{\Phi}_{i-\frac{1}{2}}^n)$$

where the notation $i + \frac{1}{2}$ corresponds to quantities estimated at the mesh interface $(i, i+1)$. R is the right-eigenvector matrix of the flux Jacobian matrix $A = \dfrac{\partial \mathbf{F}}{\partial \mathbf{q}}$. The l^{th} component of the vector $\mathbf{\Phi}_{i+\frac{1}{2}}^n$ is defined by:

$$(\phi_{i+\frac{1}{2}}^l) = \frac{1}{2}\left(|a_{i+\frac{1}{2}}^l| - \frac{\Delta t}{\Delta x}(a_{i+\frac{1}{2}}^l)^2\right)(\alpha_{i+\frac{1}{2}}^l - Q_{i+\frac{1}{2}}^l)$$

where $a_{i+\frac{1}{2}}^l$ represents the l^{th} component of the vector of local characteristic speeds, $\alpha_{i+\frac{1}{2}} = R_{i+\frac{1}{2}}^{-1}(\mathbf{q}_{i+1} - \mathbf{q}_i)$, and $Q_{i+\frac{1}{2}}^l = minmod(\alpha_{i-\frac{1}{2}}^l, \alpha_{i+\frac{1}{2}}^l, \alpha_{i+\frac{3}{2}}^l)$ is the flux limiter.

At the interface of the meshes $\mathbf{q}_{i+1/2}$ is determined by Roe's averaging, which is an approximate Riemann solver.

Steps (a) and (b) describe the classical MacCormack scheme, whereas the step (c) is a TVD flux correction. The TVD MacCormack scheme so obtained retains second-order precision in space and time in regular zones, and is oscillation-free across wave fronts. As explained by LeVeque and Yee (1990) and Garcia-Navarro et al. (1992), the main reason for choosing the predictor-corrector step instead of the one-step Lax-Wendroff formulation is that the former provides a natural way to include the source terms $\mathbf{S}$ keeping second order accuracy in time and space, whereas the one-step Lax-Wendroff scheme needs a specific treatment to do so. However, our method is limited to gently sloping beaches. For strongly varying bathymetry a "well-balanced scheme" is required (e.g. Greenberg and Leroux (1996) and Gallouët et al. (2003)).

At the seaward boundary we have implemented a method based on the fact that in the ISZ the flow is subcritical. Following Cox et al. (1994), we compute the outgoing Riemann invariant by an implicit scheme. This method allows to specify the measured water depth $h(t)$ directly at the seaward boundary of the domain $(x = 0)$. To manage the swash zone evolution we impose in dry meshes a thin water layer $h_{min} = 10^{-4}m$, with $u = 0$. Thus, NSW equations are solved everywhere in the computational domain. However, at the shoreline (wet meshes next to dry meshes) a specific treatment is applied to the discretization of the momentum equation. It consists in omitting the landward spatial differences of the horizontal hydrostatic pressure gradient, $gh\frac{\partial \zeta}{\partial x}$, in the predictor and corrector steps. Vincent et al (2001) have shown that this simple numerical treatment gives accurate results in describing shore-line evolution for a non-breaking wave climbing a beach.

C Numerical estimation of the shock-wave energy dissipation

The objective of this section is to show the ability of our shock-capturing numerical method to converge to the entropy weak solution of the NSW equations and then to compute the shock-wave energy dissipation. We present two comparisons between analytical weak solutions and numerical solutions. First, we compute the hydraulic jump associated with a dam-break on wet bottom and second we simulate the energy dissipation of a periodic broken wave on a flat bottom (see section 4 for the analytical solution). Finally, we analyze the numerical model sensivity to the spatial resolution.

Dam-break and hydraulic jump

A vertical wall is initially located at the middle of a frictionless channel. This wall separates the water with an upstream depth h_u and a downstream depth h_d (see figure 21). When the wall is removed a shock, or an hydraulic jump, occurs and reaches immediately its full strength. The analytical weak solution of this problem was developed by Stoker (1957). The constant water depth upstream the shock, h_s, is given by the implicit equation

$$2\frac{h_s}{h_d} + \left(\frac{h_s}{h_d} - 1\right)\left(\frac{1}{2}(1 + \frac{h_s}{h_d})\right)^{1/2} - 2\left(\frac{h_s}{h_d}\right)^{1/2}\left(\frac{h_u}{h_d}\right)^{1/2} = 0,$$

and the constant dimensionless energy dissipation $D_a = D_b/(\rho g(gh_d)^{1/2}h_d^2)$ is given by equation (22), which writes

$$D_a = \frac{1}{4}(\frac{h_s}{h_d} - 1)^3\left(\frac{h_s}{2h_d}(1 + \frac{h_s}{h_d})\right)^{1/2}. \tag{46}$$

In figure 21, a numerical simulation for a 100 m long channel, h_u=3m and h_d=1m, is compared with the analytical weak-solution. There is practically no distinguishable difference between analytical and computed water depth at time $t = 8$ s. The time evolution of the total energy E, integrated over the channel, is shown in figure 22. Except a small lag, due to numerical diffusion, for the first time steps of the simulation, the energy decay is in agreement with the analytical weak solution, and corresponds to the constant dissipation given by equation (46). This numerical test shows that, for hydraulic jumps, our shock-capturing method gives a numerical solution of the energy dissipation which is in agreement with the theoretical one.

Periodic wave on a flat bottom

We now investigate the behaviour of a different type of propagation, in which wave distortion proceeds continuously like in the ISZ. Figure 23 shows a comparison between the NSW numerical solution of the initial sine-wave transformation and the simple-wave solution described in section 4. The process of wave distortion, leading to the formation of a sawtooth shape profile, is correctly computed by the model. Until the shock forms at $t = t_s$, there is no distinguishable difference between analytical and computed solutions (see figure 23b). After the shock formation (see figures 23c,d), we notice that the NSW computed wave front propagates slightly faster than the simple-wave shock. This is coherent with the simple-wave hypotheses which lead to a shock velocity c_{b_s} slightly smaller than the exact NSW shock velocity c_b (see figure 3a). Figure 24 shows that the analytical energy dissipation is well reproduced by our shock-capturing method.

To assess the effect of spatial resolution on shock-wave solution, numerical simulations performed with two different mesh sizes are presented in figure 25. The two solutions are similar, excepted at the wave front where the lower resolution provides, of course, a wider front. This figure shows that the computed shock-wave kinematics is, to a great extent, independent on the spatial resolution. The time evolution of the energy dissipation computed with two different mesh sizes is presented in figure 26. We can see in this figure that the energy dissipation is weakly dependent on the resolution.

In conclusion, if the spatial mesh size is sufficiently small to describe the wave front, the numerical solution given by our TVD shock-capturing method is practically independent on the spatial resolution and converges to the NSW weak solution.

References

Battjes, J.A. 1978 Energy dissipation in breaking solitary and periodic waves. *TU Delft Report.*

Battjes, J.A. and Janssen, J.P.F.M. 1978 Energy loss and setup due to breaking of random waves. In *Proc. Int. Conf. on Coastal Eng.*, ASCE, 569-587.

Bonneton, P. 2001 A note on wave propagation in the inner surf zone, *C.R. Acad. Sci. Paris*, **329**, Série II b, 27-33.

Bonneton, P. 2004 Wave celerity in the inner surf zone. *Proc. 29th Int. Conf. on Coastal Eng.*

Bonneton, P. and Dupuis, H. 2000 Transformation of irregular waves in the inner surf zone. *Proc. 27th Int. Conf. on Coastal Eng*, **1**, 745-754.

Bonneton, P., Marieu, V., Dupuis, H., Sénéchal, N. and Castelle, B. 2005 Wave transformation and energy dissipation in the surf zone: comparison between a non-linear model and field data. *J. of Coast. Res.* SI **39**, ICS 2004, in press

Bowen, A.J., Inman, D.L. and Simmons, V.P. 1968 Wave setdown and setup. *Journal of Geophysical Research*, **73**, 2569-2577.

Buhr-Hansen, J. and Svendsen, I.A. 1979 Regular waves in shoaling water experimental data. Series Paper no. 21, ISVA, Techn. Univ. of Denmark, Lyngby.

Cox, D.T., Kobayashi, N. and Kriebel, D.L. 1994 Numerical model verification using SUPERTANK data in surf and swash zones, *proc. of Coastal Dynamics 94*, Barcelone, 248-262.

Cox, D.T. 1995 Experimental and numerical modelling of surf zone hydrodynamics, Ph.D. dissertation, Univ. of Delaware, Newark.

Dingemans, M.W., Radder, A.C. and De Vriend, H.J. 1987 Computation of the driving forces of wave-induced currents. *Coastal Engineering*, **11**, 539-563.

Dingemans, M.W. 1997 Water wave propagation over uneven bottoms. Part1 : Linear wave propagation ; Part2 : Non-linear wave propagation. *World Scientific.*

Gallouët, T., Hérard, J.-M. and Seguin, N. 2003 Some approximate Godunov schemes to compute shallow-water equations with topography. *Computers and Fluids*, **32**, 479-513.

Galvin, C.J. 1968 Breaker type classification on three laboratory beaches. *J. Geophys. Res.*, **73**, 3651-3659.

Garcia-Navarro, P., Alcrudo, F. and Saviron, J.M. 1992 1-D open channel flow simulation using TVD-McCormack scheme. *J. Hydr. Eng.*, **118**, 1359-1372.

George, R., Flick, R.E. and Guza, R.T. 1994 Observations of turbulence in the surf zone. *J. Geophys. Res.*, **99** (C1), 801-810.

Govender, K., Mocke, G.P. and Alport, M.J. 2002 Video-imaged surf zone wave and roller structures and flow fields. *J. Geophys. Res.*, **107**, 3072-3093.

Greenberg, J. and LeRoux, A.-Y. 1996 A well balanced scheme for the numerical processing of source terms in hyperbolic equations. it SIAM J. Numer. Anal., **33**, 1-16.

Hamm, L., Madsen, P.A. and Peregrine, D.H. 1993 Wave transformation in the nearshore zone: a review. *Coastal Eng.*, **21**, 5-39.

Hibbert S. and Peregrine D.H. 1979 Surf and run-up on a beach: a uniform bore, *J. Fluid Mech.*, **95**, 323-345.

Ho, D.V. and Meyer, R.E. 1962 Climb of a bore on a beach. Part 1: Uniform beach slope. *J. Fluid Mech.*, **14**, 305-318.

Johnson, R.S. 1997 A modern introduction to the mathematical theory of water waves. *Cambridge University Press.*

Keller, H.B., Levine, D.A. and Whitham, G.B. 1960 Motion of a bore over a sloping beach. *J. Fluid Mech.*, **7**, 302-316.

Kennedy, A.B., Chen, Q., Kirby, J.T. and Dalrymple, R.A. 2000 Boussinesq modeling of wave transformation, breaking and runup. I: one. *J. Waterway, Port Coastal and Ocean Engineering*, **126** (1), 39-47.

Kobayashi, N. and Watson, K. D. 1987 Wave Reflection and Runup on Smooth

Slopes. *Proceedings of Coastal Hydrodynamics*, ASCE, 548-563.

Kobayashi, N., DeSilva, G.S. and Watson, K.D. 1989 Wave transformation and swash oscillation on gentle and steep slopes. *J. Geophys. Res.* **94** (C1), 951-966.

Kobayashi, N., Cox, D.T. and Wurjanto, A. 1990 Irregular wave reflection and run-up on rough impermeable slopes. *Journal of Waterway, Port, Coastal, and Ocean Engineering*, **116**, 708-728.

Kobayashi, N. and Karjadi, E. A. 1996 Obliquely incident irregular waves in surf and swash zones, *J. Geophys. Res.*, **101** (C3), 6527-6542.

Le Méhauté, B. 1962 On the non-saturated breaker theory and the wave run-up. *Proc. 8th Coastal Engineering Conf.* 77-92.

LeVeque, R.J. and Yee, H.C. 1990 A study of numerical methods for hyperbolic conservation laws with stiff source terms. *J. Comput. Phys.*, **86**, 187-210.

LeVeque, R.J. 1992 Numerical Methods for Conservation Laws. *Birkhauser Verlag*, Boston.

Lin, P. and Liu, P. L.-F. 1998 A numerical study of breaking waves in the surf zone, *J. Fluid Mech.*, **359**, 239-264.

Liu, P. L.-F., Synolakis, C.E. and Yeh, H.H. 1991 Report on the International Workshop on Long-Wave Run-up, *J. Fluid Mech.*, **229**, 675-688.

Longuet-Higgins, M.S. and Stewart, R.W. 1964 Radiation stress in water waves, a physical discussion with application. *Deep Sea Res.*, **11**, 529-563.

Longuet-Higgins, M.S. 1973 The mechanics of the surfzone. *Proc. 13th Int. Congress of Theoretical and Applied Mechanics*, Moscow, Springer Verlag, 213-228.

Madsen, P.A., Sorensen, O.R. and Schäffer, H.A. 1997 Surf zone dynamics simulated by a Boussinesq type model. Part I. Model description and cross-shore motion of regular waves. *Coastal Eng.*, **32**, 255-287.

Mei, C.C. 1989 The applied dynamics of ocean surface waves. *World Scientific.*

Nadaoka, K., M. Hino and Y. Koyano, 1989 Structure of the turbulent flow field under breaking waves in the surf zone. Journal of Fluid Mechanics, **204**, 359-387.

Ozanne, F., Chadwick, A.J., Huntley, D.A., Simmonds, D.J. and Lawrence, J. 2000 Velocity predictions for shoaling and breaking waves with a Boussinesq-type model. *Coastal Eng.*, **41**, 361-397.

Peregrine, D. H. 1967 Long waves on a beach. Journal of Fluid Mechanics, **27**, 815-827.

Peregrine, D. H. 1983 Breaking waves on beaches. Annual Review of Fluid Mechanics, **15**, 149-178.

Peronnard, C. and Hamm, L. 1995 Database waves and associated currents for coastal profile modelling (release 1.1). *Report SOGREAH* n°52184R6, prepared for G8M Coastal Morphodynamics european project n° MS2-CT92-0027, Grenoble, France.

Phillips, O.M. 1977 The dynamics of the upper ocean. Second edition. Cambridge University Press.

Raubenheimer, B., Guza, R.T. and Elgar, S. 1996 Wave transformation across the inner surf zone. *J. Geophys. Res.* **101** (C10), 25589-25597.

Schäffer, H.A., Madsen, P.A. and Deigaard, R. 1993 A Boussinesq model for waves breaking in shallow water. *Coastal Eng.*, **20**, 185-202.

Sénéchal, N., Dupuis, H., Bonneton, P., Howa, H. et Pedreros, R. 2001 Observation of irregular wave transformation in the surf zone over a gently slopping sandy beach, *Oceanologica Acta*, **24** (6), 545-556.

Serre, D. 1996 Systèmes de lois de conservation, Partie I. *Diderot Editeur.*

Shen, M.C. and Meyer, R.E. 1963 Climb of a bore on a beach. Part 3: Run-up. *J. Fluid Mech.*, **16**, 113-125.

Stive, M.J.F. 1984 Energy dissipation in waves breaking on gentle slopes. *Coast. Eng.* **8**, 99-127.

Stoker, J.J., 1957 Water Waves, Interscience Publishers, New York.

Svendsen, I. A. 1987 Analysis of surf zone turbulence. *J. Geophys. Res.*, **92** (C5), 5115-5124.

Svendsen, I.A., Madsen, P.A. and Hansen, J.B. 1978 Wave characteristics in the surf zone. *Proc. 16th Coastal Engineering Conf.*, 520-539.

Svendsen, I.A., Qin, W. and Ebersole, B.A. 2003 Modelling waves and currents at the LSTF and other laboratory facilities. *Coastal Eng.*, **50**, 19-45.

Tega, Y. and Kobayashi, N. 2002 Sediment transport in wave uprush and downrush on swash zone. *Proc. 28th Coastal Engineering Conf.*, 993-1005.

Thornton, E.B. and Guza, R.T. 1982 Energy saturation and phase speeds measured on a natural beach. *J. Geophys. Res.*, **87**, 9499-9508.

Thornton, E.B. and Guza, R.T. 1983 Transformation of wave height distribution. *J. Geophys. Res.*, **88**, 5925-5938.

Ting, F.C.K. and Kirby, J.T. 1996 Dynamics of surf-zone turbulence in a spilling breaker. *Coastal Eng.*, **27**, 131-160.

Vincent, S., Bonneton, P. and Caltagirone, J-P. 2001 Numerical modelling of bore propagation and run-up on sloping beaches using a MacCormack TVD scheme, *J. of Hydr. Research*, **39**, 41-49.

Whitham, G.B. 1958 On the propagation of shock waves through regions of non-uniform area or flow. *J. Fluid Mech.* **4**, 337-360.

Whitham, G.B. 1974 Linear and nonlinear Waves. *Wiley-Interscience Publication.*

Yee, H.C. 1987 Upwind and Symmetric Shock-Capturing Schemes, NASA Technical Memorandum, 89464.

Figure captions

Figure 1: Definition sketch. a, cross-section of a broken-wave in the ISZ (RWR, regular wave region; WF, wave front); b, shock-wave representation. c_b is the broken-wave celerity, H the wave height, h the water depth and subscript 1 and 2 indicate values respectively ahead and behind the shock.

Figure 2: Surface elevation and velocity data in the ISZ from Cox (1995); $d_0 = 7.43$ cm, $a_0 = H_0/2 = 2.52$ cm, $T = 2.2$ s and $\beta = 1/35$. a, temporal variations of nondimensional phase-averaged free surface elevation $\langle\zeta\rangle/a_0$; b, vertical variations of nondimensional phase-averaged horizontal velocity $\langle v_1\rangle/\mathcal{U}$. $\bullet$, measured velocity; ______, depth-averaged velocity; $- \cdot - \cdot -$, free surface elevation.

Figure 3: Relative errors of the simple-wave shock velocity c_{b_s} and dissipation D_{b_s} compared to the exact shock velocity c_b and dissipation D_b, as a function of the shock strength ϵ. a, $(c_b - c_{b_s})/c_{b_s}$; b, $(D_b - D_{b_s})/D_{b_s}$.

Figure 4: Dimensionless energy dissipation $D_a = D_{b_s}/(\rho g c_0 d_0^2)$ of a sine wave ($\epsilon_0 = 0.3$), as a function of time.

Figure 5: Multi-valued solution and equal area construction for the position of the shock.

Figure 6: Schematic view of the experimental setup, Cox (1995), and the computational domain. $\beta = 1/35$, $T = 2.2$ s and $H_w = 0.115$ m. Four measurement

cross-sections are located in the ISZ: L1 ($x = 0$ m, $d = 0.1771$ m); L2 ($x = 1.2$ m, $d = 0.1429$ m); L3 ($x = 2.4$ m, $d = 0.1086$ m); L4 ($x = 3.6$ m, $d = 0.0743$ m). The computational domain starts at $x = 0$ m, where the seaward boundary condition is given by time series of water depth at L1.

Figure 7: Time series of surface elevation in the inner surf zone. Comparison between NSW numerical model (dashed line) and experiments by Cox (1995) (solid line). a, L1 ($x = 0$ m, $d = 0.1771$ m); b, L2 ($x = 1.2$ m, $d = 0.1429$ m); c, L3 ($x = 2.4$ m, $d = 0.1086$ m); d, L4 ($x = 3.6$ m, $d = 0.0743$ m).

Figure 8: Comparison between computed wave front trajectories and experimental wave front positions. NSW model (solid line); c_{b1} model (long-dashed line); c_{b2} model (short-dashed line); experimental data from Cox (1995) ($\times$).

Figure 9: Spatial evolution of wave elevation. Comparison between the NSW numerical model and experiments by Cox (1995). Computed ζ_{min} and ζ_{max} (short-dashed lines); computed $\bar{\zeta}$ (long-dashed line); instantaneous surface elevation at a given time t_i (solid line); measured ζ_{min} and ζ_{max} ($\diamond$); measured $\bar{\zeta}$ ($*$).

Figure 10: Spatial evolution of wave elevation. Comparison between the NSW numerical model and experiments by Ting and Kirby (1996) ($\beta = 1/35$, $T = 2$ s and $H_w = 0.125$ m). Computed ζ_{min} and ζ_{max} (short-dashed lines); computed $\bar{\zeta}$ (long-dashed line); instantaneous surface elevation (solid line); measured ζ_{min} and ζ_{max} ($\diamond$); measured $\bar{\zeta}$ ($*$).

Figure 11: Vertical structure of the phase-averaged horizontal velocity $\langle v_1 \rangle$ at L3. $\bullet$, measured velocity (Cox (1995)) ; ____, depth-averaged measured velocity u_m ; $---$, computed depth-averaged velocity u ; $- \cdot - \cdot -$, free surface position. a, $t = t_*$; b, $t = t_* + T/6$; c, $t = t_* + 2T/6$; d, $t = t_* + 3T/6$; e, $t = t_* + 4T/6$; f, $t = t_* + 5T/6$.

Figure 12: Time series of depth-averaged velocity in the inner surf zone. Comparison between NSW computed velocity u (dashed line) and u_m estimated from the data of Cox (1995) (solid line). a, L1 ($x = 0$ m, $d = 0.1771$ m); b, L2 ($x = 1.2$ m, $d = 0.1429$ m); c, L3 ($x = 2.4$ m, $d = 0.1086$ m); d, L4 ($x = 3.6$ m, $d = 0.0743$ m).

Figure 13: NSW computed Riemann invariant $\alpha^- = u - 2c$ divided by $\bar{u} - 2\bar{c}$, at a given time t_i (see the surface elevation in figure 9), as a function of x.

Figure 14: Spatial evolution of wave elevation. Comparison between the one-way model and experiments by Cox (1995). Computed ζ_{min} and ζ_{max} (short-dashed lines); computed $\bar{\zeta}$ (long-dashed line); instantaneous surface elevation at a given time t_i (solid line); measured ζ_{min} and ζ_{max} ($\diamond$); measured $\bar{\zeta}$ ($*$) ; NSW instantaneous surface elevation at t_i (dot-dashed line).

Figure 15: Spatial evolution of wave elevation. Comparison between the one-way model and experiments by Ting and Kirby (1996) ($\beta = 1/35$, $T = 2$ s and $H_w = 0.125$ m). Computed ζ_{min} and ζ_{max} (short-dashed lines); computed $\bar{\zeta}$ (long-dashed line); instantaneous surface elevation (solid line); measured ζ_{min} and ζ_{max}

($\diamond$); measured $\bar{\zeta}$ ($*$); NSW instantaneous surface elevation (dot-dashed line).

Figure 16: Comparison between computed wave front trajectories and experimental wave front positions. NSW model (solid line); one-way model (dashed line); experimental data from Cox (1995) ($\times$).

Figure 17: Measured and computed cross-shore variations of the potential energy E_p. Cox (1995) experiment ($*$); NSW model (solid line); one-way model (dashed line).

Figure 18: Cross-shore variations of the wave setup. Comparisons between NSW numerical model (solid line) and experiments by Buhr-Hansen and NSWendsen (1979)($\diamond$). $\beta = 1/34.26$, $T = 1.452$ s and $H_w = 0.0943$ m.

Figure 19: Measured and computed cross-shore variations of the wave setup. Ting and Kirby (1996) experiment ($*$); NSW numerical model (solid line); one-way model (dashed line).

Figure 20: Classical analogy between broken-wave and hydraulic jump. h is the water depth and subscript 1 and 2 indicate values respectively ahead and behind the wave front. c_b is the broken-wave velocity

Figure 21: Comparison between computed water depth profile (short-dashed line) and analytical weak-solution (solid line) of the dam-break problem at $t = 8$ s. Initial condition (long-dashed line): $h_d = 1$ m, $h_u = 3$ m. Numerical parameters: $\Delta x = 0.1$ m, $\Delta t = 0.01$ s.

Figure 22: Time evolution of wave energy $(E_0 - E)/E_0$ for the dam-break problem ($E_0 = E(t = 0)$). Comparison between analytical weak-solution (solid line) and numerical solution (short-dashed line). Initial condition: $h_d = 1$ m, $h_u = 3$ m. Numerical parameters: $\Delta x = 0.1$ m, $\Delta t = 0.01$ s.

Figure 23: Comparison between analytical simple-wave solution (solid line) and numerical solution (short-dashed line) of the initial sine wave ($\epsilon_0 = 0.3$) transformation in the moving coordinate system $x_1 = x - c_0 t$. Numerical parameters: $\Delta x/\lambda_0 = 2\,10^{-3}$, $\Delta t/(c_0\lambda_0) = 6.4\,10^{-5}$. a, $t/t_s = 0$; b, $t/t_s = 1$; c, $t/t_s = 1.2$; d, $t/t_s = 2$.

Figure 24: Time evolution of the dimensionless energy dissipation $D_a = D_{b_s}/(\rho g c_0 d_0^2)$. Comparison between analytical simple-wave solution (solid line) and numerical solution (short-dashed line) of the initial sine wave ($\epsilon_0 = 0.3$) transformation. Numerical parameters: $\Delta x/\lambda_0 = 2\,10^{-3}$, $\Delta t/(c_0\lambda_0) = 6.4\,10^{-5}$.

Figure 25: Numerical solutions of the initial sine wave ($\epsilon_0 = 0.3$) transformation in the moving coordinate system $x_1 = x - c_0 t$, at $t/t_s = 2$ with $\Delta t/(c_0\lambda_0) = 6.4\,10^{-5}$. Dashed line, $\Delta x/\lambda_0 = 2\,10^{-3}$; short-dashed line, $\Delta x/\lambda_0 = 10^{-2}$.

Figure 26: Time evolution of the dimensionless energy dissipation $D_a = D_{b_s}/(\rho g c_0 d_0^2)$, for two different spatial resolutions. Dashed line, $\Delta x/\lambda_0 = 2\,10^{-3}$; short-dashed line, $\Delta x/\lambda_0 = 10^{-2}$.

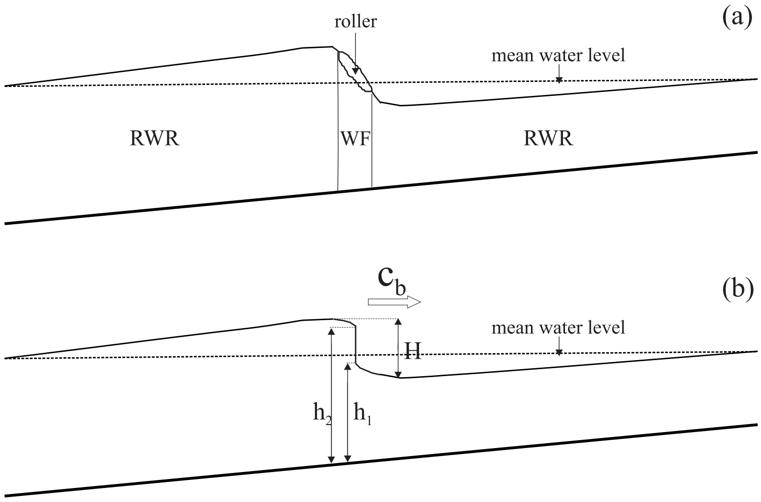
(a)
roller
mean water level
RWR
WF
RWR
(b)
c_b
mean water level
H
h_2
h_1

a

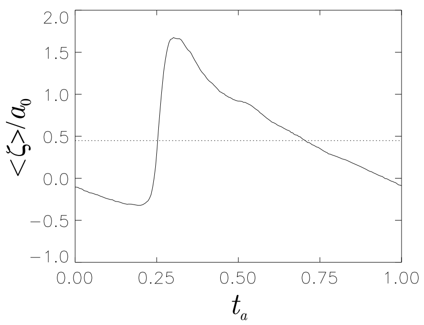

b

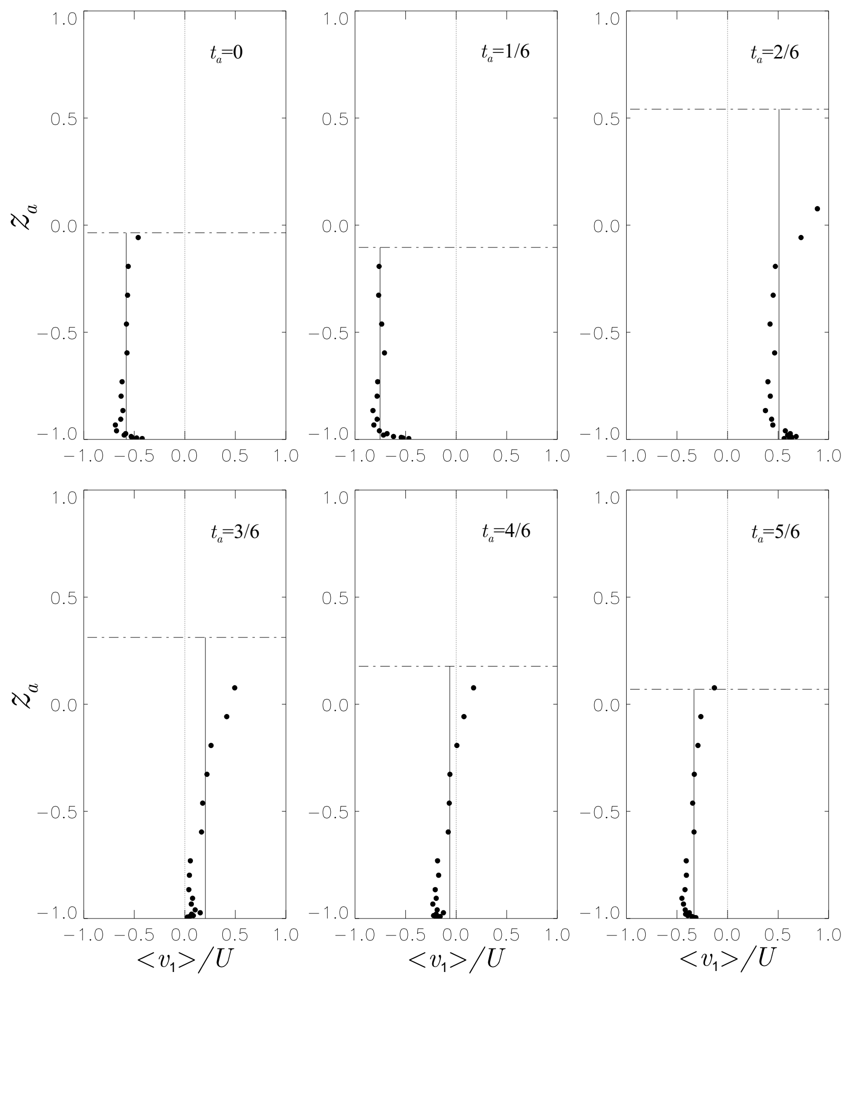

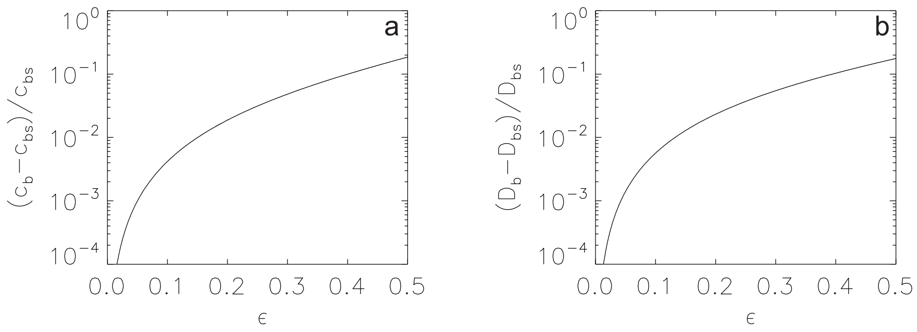
a
b
$(c_b - c_{bs})/c_{bs}$
$(D_b - D_{bs})/D_{bs}$
10^0
10^{-1}
10^{-2}
10^{-3}
10^{-4}
0.0 0.1 0.2 0.3 0.4 0.5
ϵ

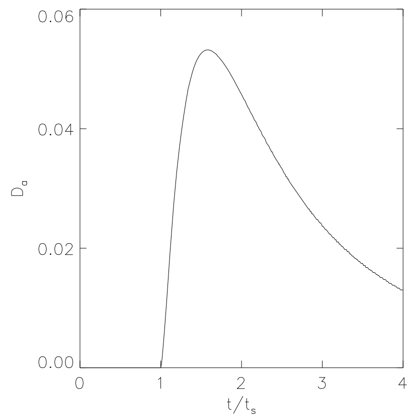
0.06
0.04
0.02
0.00
D_a
0
1
2
3
4
t/t_s

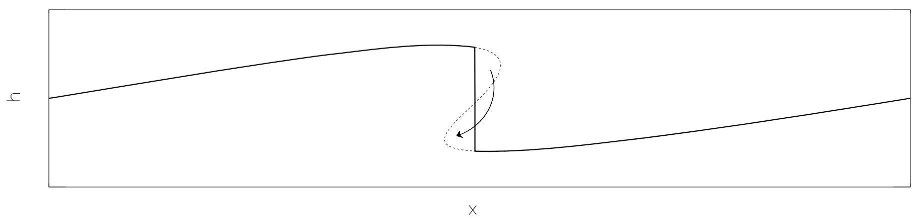
h
x

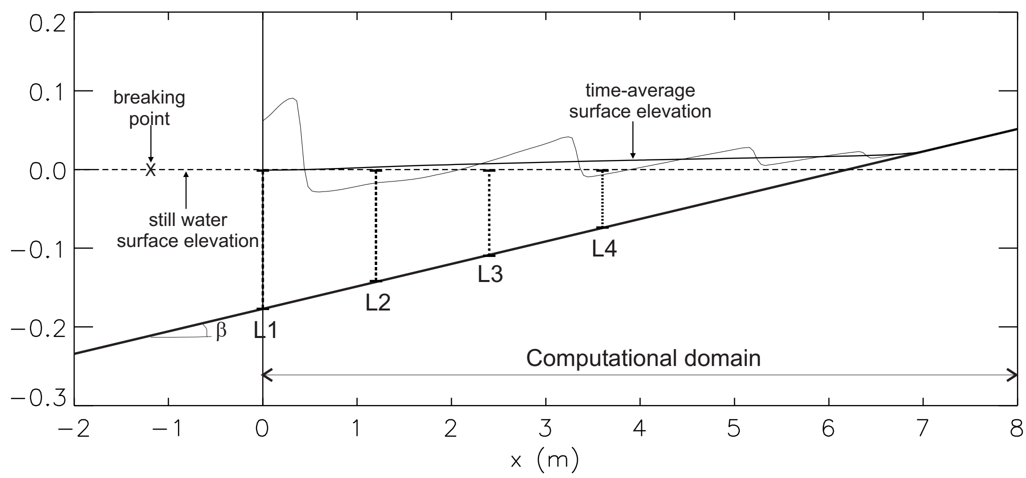

0.2
0.1
0.0
−0.1
−0.2
−0.3
z (m)
breaking point
time-average surface elevation
still water surface elevation
L1
L2
L3
L4
β
Computational domain
−2
−1
0
1
2
3
4
5
6
7
8
x (m)

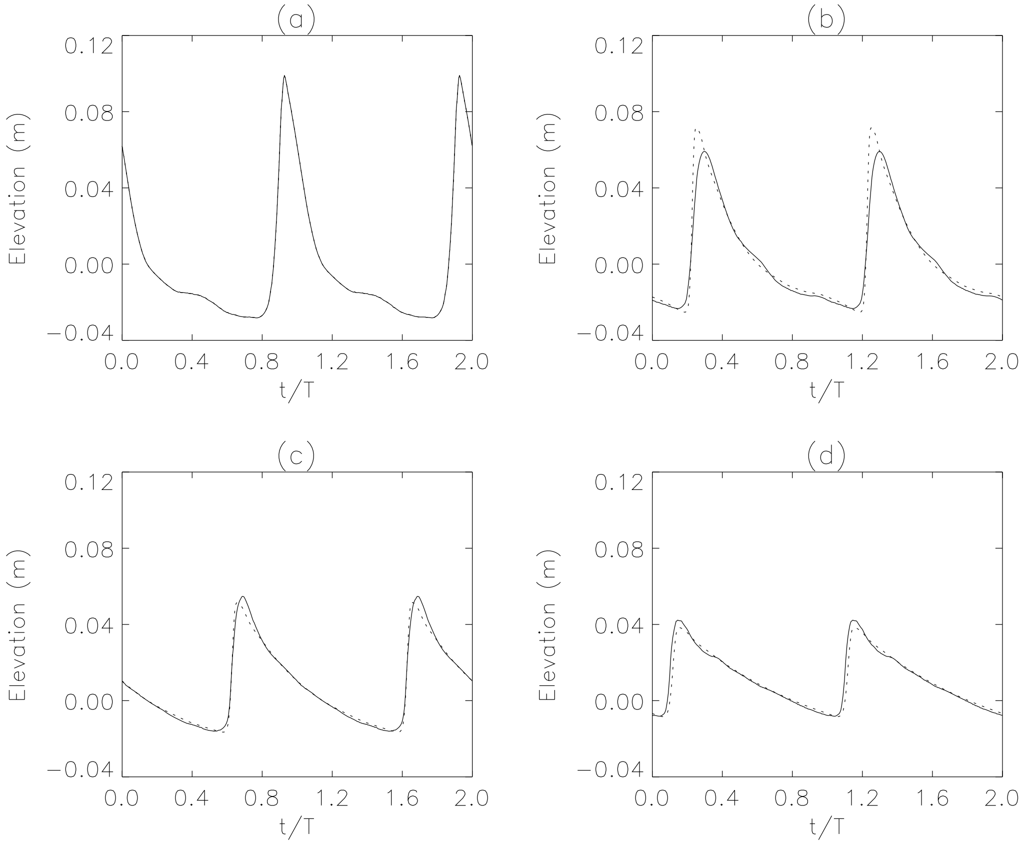
(a)
(b)
(c)
(d)
Elevation (m)
t/T
0.12
0.08
0.04
0.00
−0.04
0.0
0.4
0.8
1.2
1.6
2.0

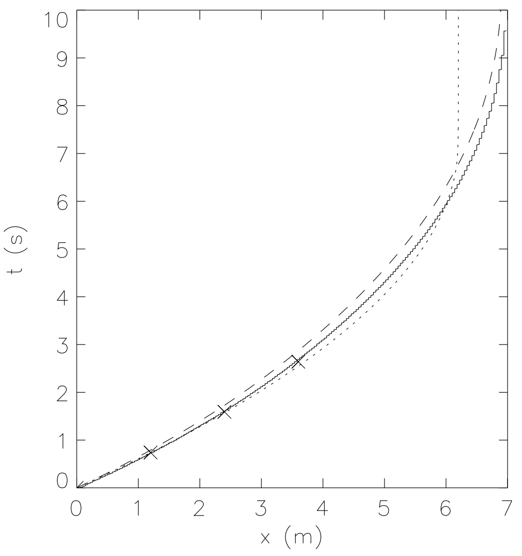

t (s)
x (m)
0
1
2
3
4
5
6
7
8
9
10

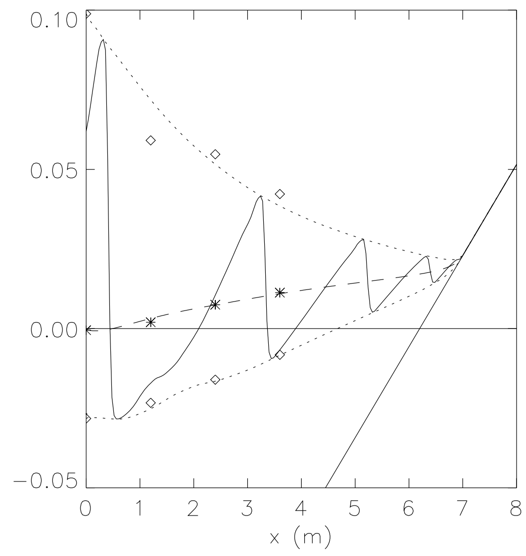
0.10
0.05
0.00
−0.05
z (m)
0
1
2
3
4
5
6
7
8
x (m)

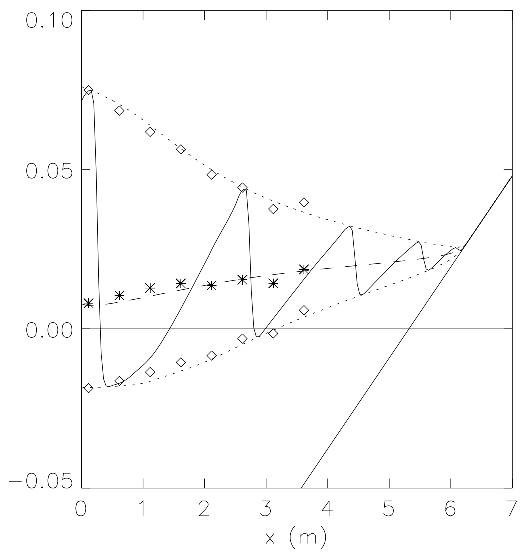
0.10
0.05
0.00
−0.05
z (m)
0
1
2
3
4
5
6
7
x (m)

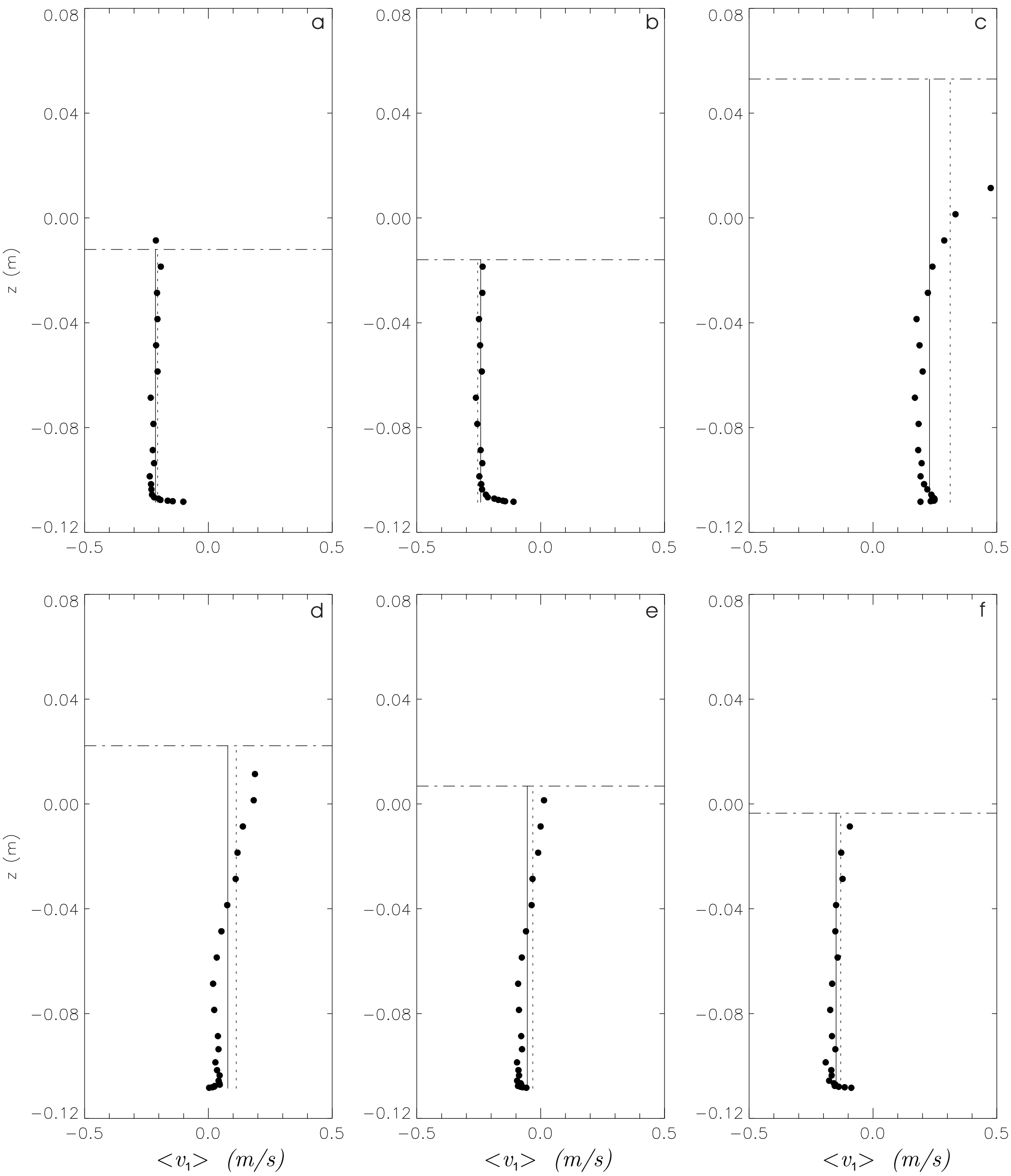

a
b
c
d
e
f
z (m)
0.08
0.04
0.00
−0.04
−0.08
−0.12
−0.5
0.0
0.5
$<v_1>$ (m/s)

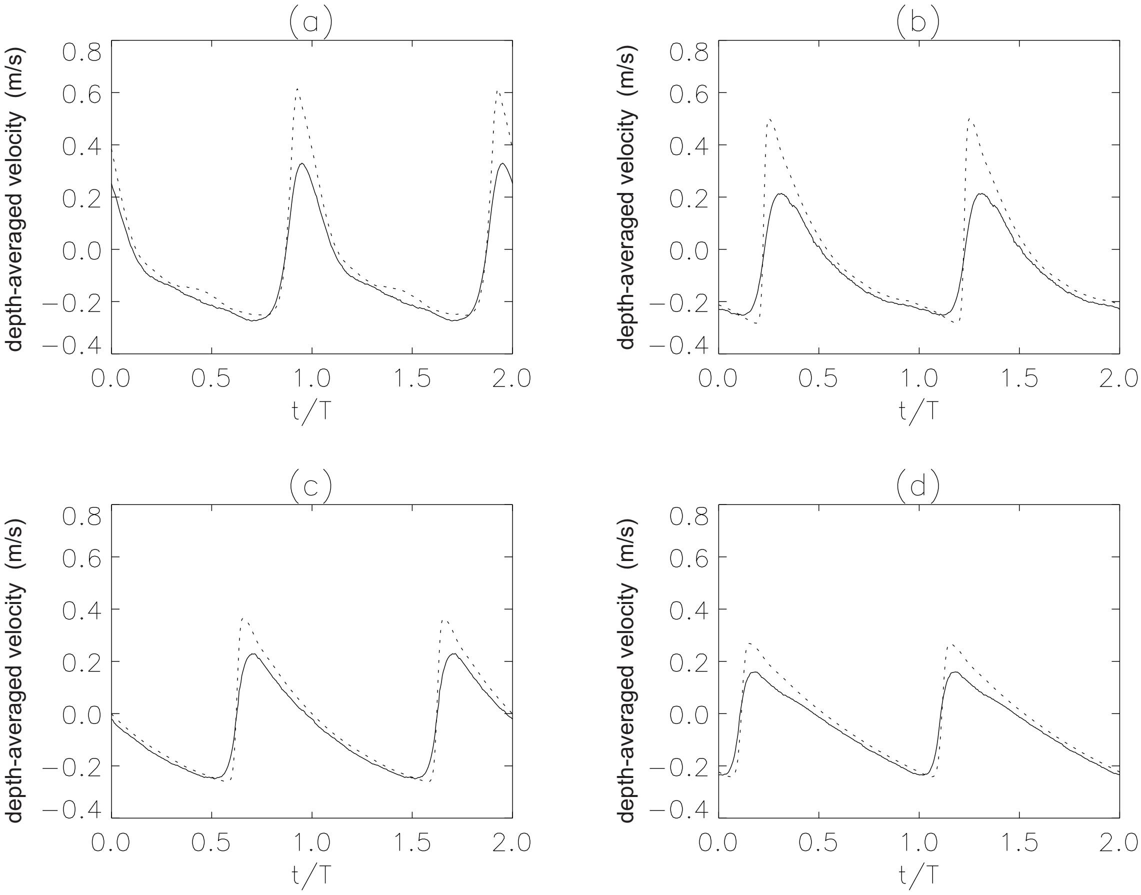

(a)
(b)
(c)
(d)
depth-averaged velocity (m/s)
0.8
0.6
0.4
0.2
0.0
−0.2
−0.4
0.0
0.5
1.0
1.5
2.0
t/T

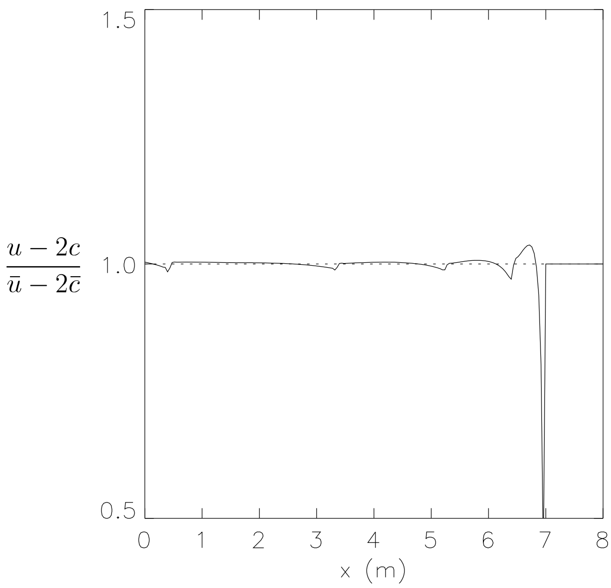

1.5
1.0
0.5
0
1
2
3
4
5
6
7
8
x (m)

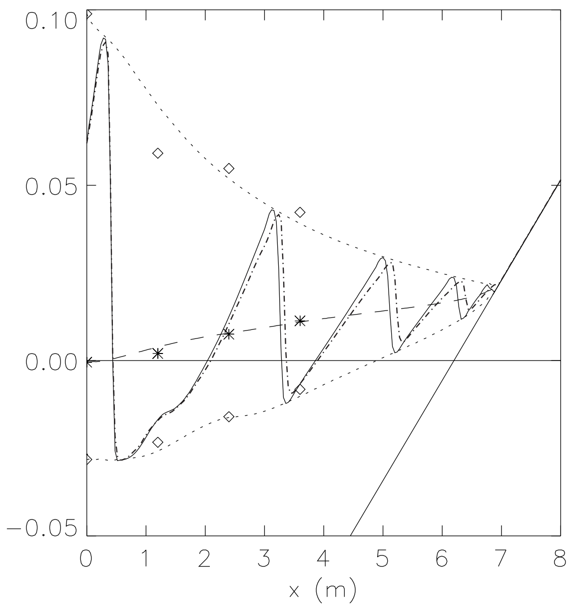

0.10
0.05
0.00
−0.05
z (m)
0
1
2
3
4
5
6
7
8
x (m)

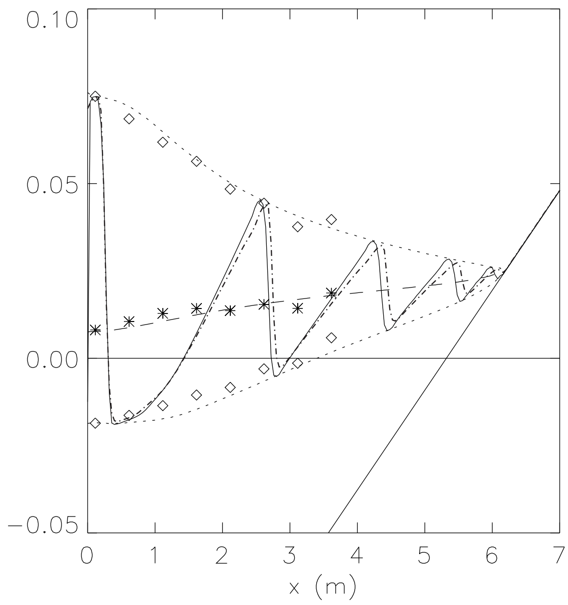

0.10
0.05
0.00
−0.05
z (m)
0
1
2
3
4
5
6
7
x (m)

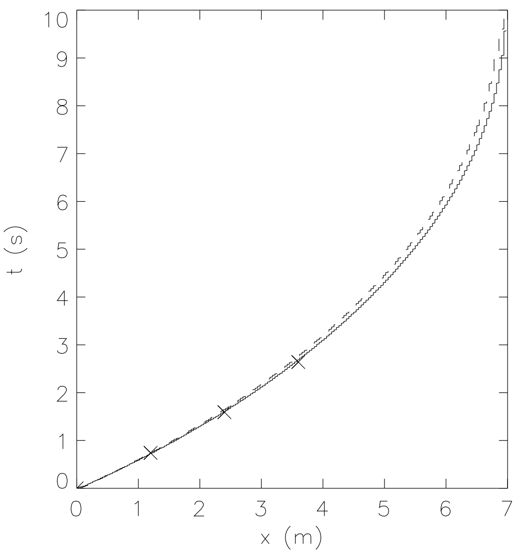

10
9
8
7
6
5
4
3
2
1
0
t (s)
0
1
2
3
4
5
6
7
x (m)

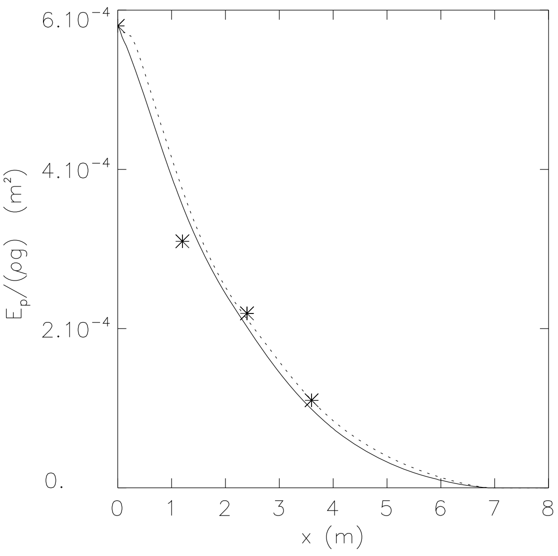

6.10⁻⁴
4.10⁻⁴
2.10⁻⁴
0.
$E_p/(\rho g)$ (m²)
0 1 2 3 4 5 6 7 8
x (m)

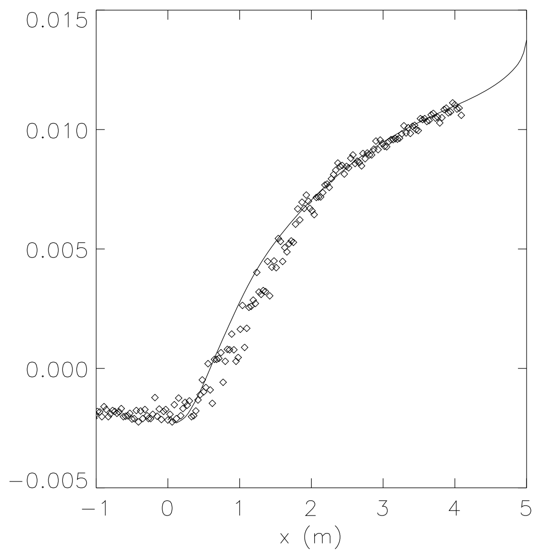
0.015
0.010
0.005
0.000
−0.005
−1
0
1
2
3
4
5
x (m)

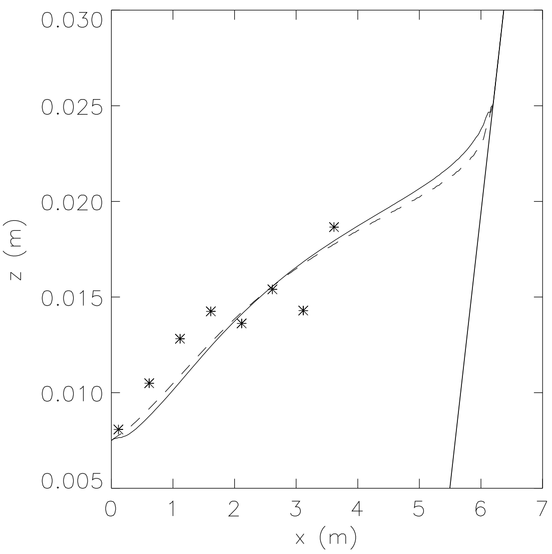

0.030
0.025
0.020
0.015
0.010
0.005
z (m)
0
1
2
3
4
5
6
7
x (m)

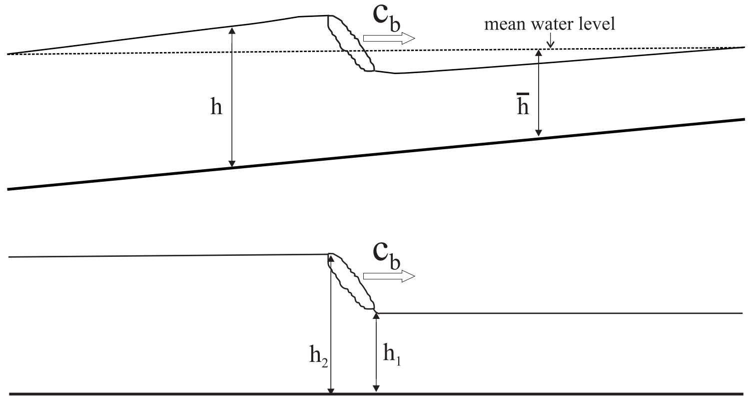

c_b
mean water level
h
$\bar{h}$
c_b
h_2
h_1

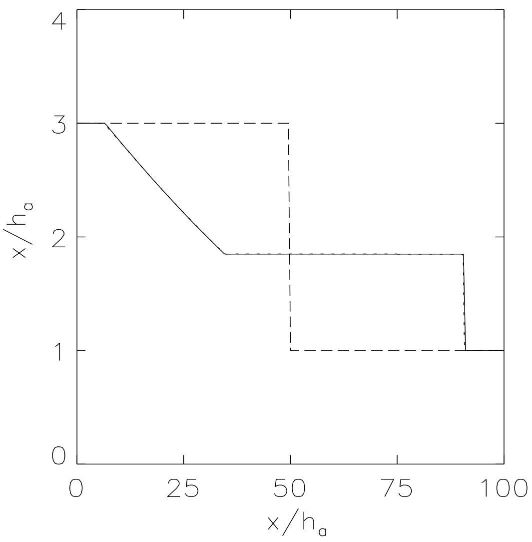

4
3
2
1
0
x/h_a
0
25
50
75
100
x/h_a

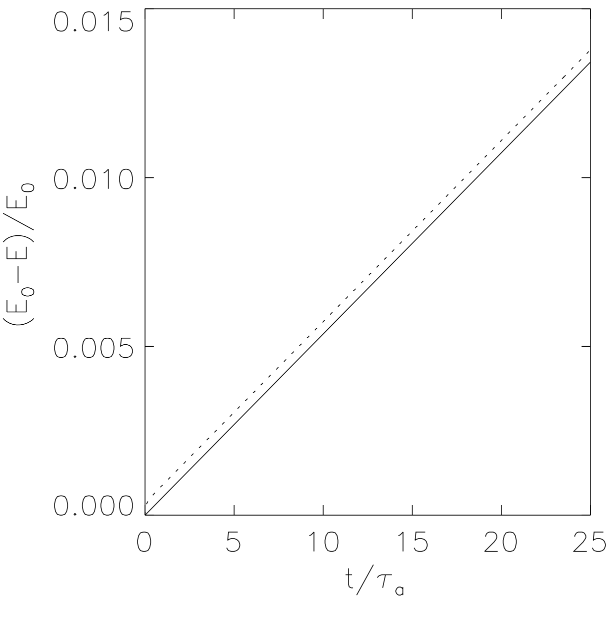

0.015
0.010
0.005
0.000
$(E_0 - E)/E_0$
0
5
10
15
20
25
t/τ_a

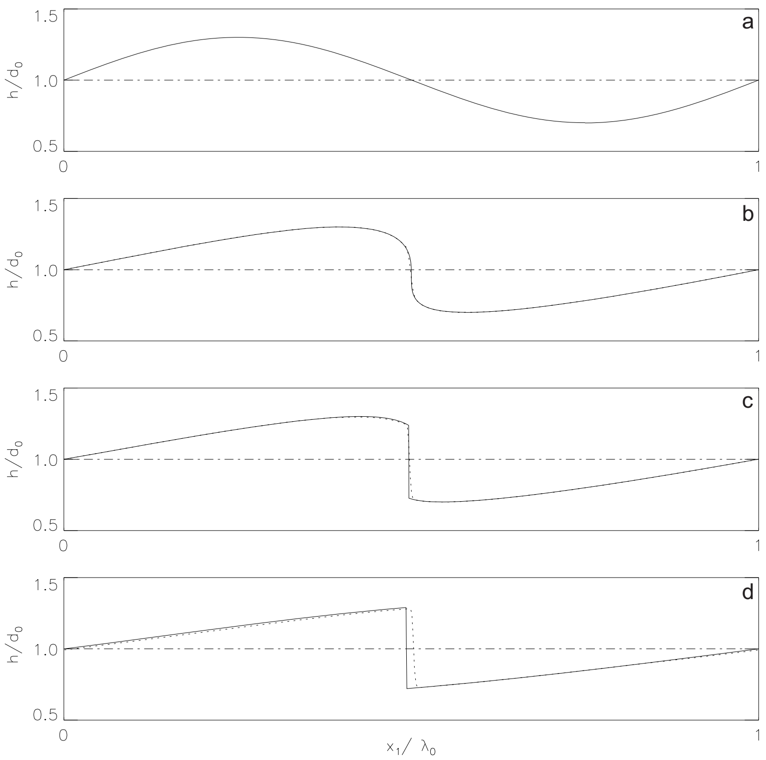

a
b
c
d
h/d0
1.5
1.0
0.5
0
1
x1/ λ0

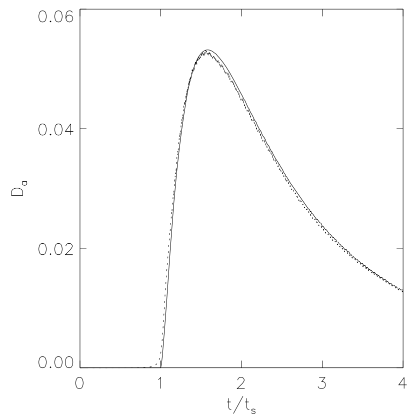

0.06
0.04
0.02
0.00
D_a
0
1
2
3
4
t/t_s

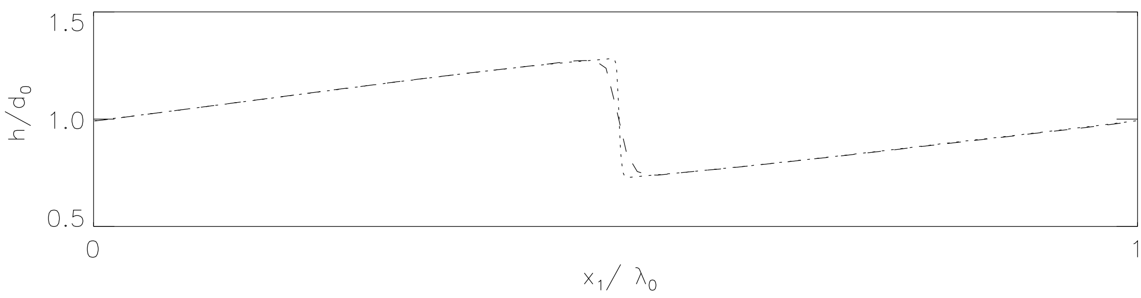
1.5
1.0
0.5
h/d0
0
1
x1/ λ0

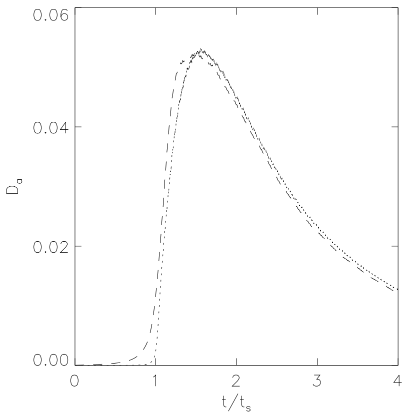
0.06
0.04
0.02
0.00
D_a
0
1
2
3
4
t/t_s